Title
PRODUCTION CROSS SECTIONS FOR POSITIVE AND NEGATIVE PIONS FROM CARBON INITIATED BY 340-MeV PROTONS

Author
Dudziak, Walter Francis.

Publication Date
1954-04-01

UNIVERSITY OF
CALIFORNIA

Radiation Laboratory

BERKELEY, CALIFORNIA

DISCLAIMER

UCRL-2564
Unclassified-Physics Distribution

UNIVERSITY OF CALIFORNIA
Radiation Laboratory

Contract No. W-7405-eng-48

PRODUCTION CROSS SECTIONS FOR POSITIVE AND NEGATIVE PIONS FROM CARBON INITIATED BY 340-MEV PROTONS

Walter Francis Dudziak

(Thesis)

April 1954

Berkeley, California

Contents

Abstract 4

I. Introduction 5

II. General Description of the Experiment 7

III. Details of Experimental Procedure

A. Proton Source and Collimation 9

B. Experimental Studies with a Uniform Magnetic Field (Pair Magnet)

1. Detailed Description of Experimental Method . . . 9

2. Magnetic Field and Channel 12

3. Targets 14

4. Pion Detection 15

5. Calculation of the Cross Section. 21

6. Experimental Results

a. Cross sections for positive pions

1. π^+ Spectrum at 0° to proton beam 24

2. π^+ Spectrum at 90° to proton beam 27

b. Cross sections for negative pions

1. Prong distribution 27

2. π^- Spectrum at 0° to proton beam 33

c. Charged-pion production ratios at 0° to the proton beam 33

C. Experimental Studies with a 22-inch Spiral-Orbit Spectrometer

1. Some Facts Concerning the Spiral-Orbit Principle .38

2. Detailed Description of Experimental Method . . .41

a. Magnet and experimental procedure 41

b. Properties of a spiral-orbit spectrometer having a particular geometry: pion detection . .45

3. Experimental Results on Pion Production at 90° to Proton Beam 56

IV. Discussion

A. Production of Positive Pions from Carbon at 90° to the Proton Beam 65

B. Production of Negative Pions at 90° to the Proton Beam .72

C. Our Present Knowledge about Charged-Pion Production from Carbon by 340-Mev Protons 75

Acknowledgements 82
Appendix 83
References 90

PRODUCTION CROSS SECTIONS FOR POSITIVE AND NEGATIVE PIONS FROM CARBON INITIATED BY 340-MEV PROTONS

Walter Francis Dudziak

Radiation Laboratory, Department of Physics,
University of California, Berkeley, California

April 1954

ABSTRACT

Production of π^+ and π^- at 0° and 90° to a 340-Mev proton beam has been studied with nuclear emulsions in both uniform and heterogeneous magnetic fields. Conclusions are:

(a) the peak of the cross section for π^- production at these laboratory angles is at a much lower energy than for π^+ production;

(b) the maximum pion-energy cutoff for π^- production is smaller than for π^+ production;

(c) the shapes of the π^--production spectrum disagree with those previously reported, particularly at low pion energies;

(d) at low energies the plots of $\pi^\pm$ cross sections against pion energy qualitatively resemble corresponding $\beta^\pm$ decay spectra;

(e) integrating these spectra over the pion energy gives

Angle (lab)	$\frac{d\sigma^+}{d\Omega}$ x 10^{28} $cm^2\,ster^{-1}$	$\frac{d\sigma^-}{d\Omega}$ x 10^{28} $cm^2\,ster^{-1}$	$\frac{\pi^+}{\pi^-}$	$\frac{\pi^+(0^\circ)}{\pi^+(90^\circ)}$	$\frac{\pi^-(0^\circ)}{\pi^-(90^\circ)}$
0°	21.0 ± 0.5	0.71 ± 0.02	29.5 ± 1.2	6.3 ± 0.2	1.67 ± 0.09
90°	3.35 ± 0.07	0.43 ± 0.02	7.8 ± 0.4		

(f) with the aid of Leonard's 180° results on $\pi^\pm$ from carbon an estimate is made of the total production cross section per C nucleus: $\sigma_T^+ = (7.6 \pm 0.7) \times 10^{-27} cm^2$; $\sigma_T^- = (0.55 \pm 0.09) \times 10^{-27} cm^2$; $\pi^+/\pi^- = 14 \pm 4$;

(g) the disagreement between previously published data on π^+ production at 90° is resolved for pion energies above 25 Mev;

(h) for the calculation of the π^--production cross section a more appropriate zero-prong correction is 1.35;

(i) the spiral-orbit principle is especially suited to the study of charged-pion production at 90° to the proton beam.

PRODUCTION CROSS SECTIONS FOR POSITIVE AND NEGATIVE PIONS FROM CARBON INITIATED BY 340-MEV PROTONS

Walter Francis Dudziak

Radiation Laboratory, Department of Physics,
University of California, Berkeley, California

April 1954

I. INTRODUCTION

Among the many interesting experiments that will aid in the development of meson theories is the measurement of cross sections for pion production resulting from inelastic collisions between free nucleons. There are of course three such problems, these being the measurement of pion production from a free proton-proton interaction, from a proton-neutron interaction, and from a neutron-neutron interaction. A subtraction technique has been successfully applied in the study of the proton-proton interaction,[1,2] and also in the study of the proton-neutron interaction.[3] Since for the p-p case a polyethylene target, $(CH_2)_n$, is used, and for the p-n case a deuterated polyethylene target, $(CD_2)_n$, is used, a detailed study must be made of pion production from carbon, at least over the pion energy region defined by the conservation laws when these are applied to the problem of pion creation in free nucleon-nucleon collision.

Extension of these studies of pion production from carbon at 0^o to the proton beam was prompted by the fact that, in a preliminary survey[4] of charged-pion production from carbon, much larger positive-to-negative pion ratios were observed than were predicted by the (A+Z)/(A-Z) ratio or by earlier production studies from complex nuclei[5] at 90^o to the proton beam. The (A+Z)/(A-Z) ratio would be expected, at least for pions in an energy interval where the nuclear Coulomb barrier effect can be neglected, if the protons and neutrons in the carbon nucleus had equal cross sections for pion production and if the $(p\text{-}n, \pi^+)$ reaction had the same probability as the $(p\text{-}n, \pi^-)$ reaction. Although a variation of this ratio was predicted on grounds of the Pauli principle,[6] nevertheless, the observed preliminary data disclosed that the production of negative pions by incident protons was suppressed more strongly

than the Pauli argument, as presented, would indicate.

The stimulus for the studies of pion production from carbon at 90° to the proton beam was the ingenious principle of large solid-angle focusing first proposed by Miyamoto[7] and developed principally by Miyamoto,[8,9,10] Sagane,[10] Iwata,[9] Kotani,[9] and Sakai.[11] The principle, now commonly referred to as the "Spiral-Orbit Principle", was first introduced to this country by Sagane.[12,13] The purpose of the principle as applied to the study of charged-pion production[13] was the accurate determination of π^+/π^- ratios from complex nuclei. The principle was not applied to measurement of pion-production cross sections because of the forbidding complexity of calculating the variation of the solid angle in a study of charged-pion production when pion energies exceed the stable-orbit energy. An experimental method was proposed[3] to surmount this dilemma. This is discussed in Section III.

The choice of carbon for the study of the solid-angle variation was chiefly because of the π^+ -production data obtained in earlier experiments[5,2] on this element at 90° to the proton beam. However, it was found not only that the π^+ data as reported were inconsistent between the two experiments, but also that the two expressions, as they were used for the calculation of these cross sections, were generally in disagreement.[14,15] As a result a more refined experimental study was made on π^+ production from carbon at 90° to the proton beam.

A possible way of resolving the difference between the two methods of calculating the cross section is also discussed. An application of the proposed calculations results generally in good agreement of all experimental measurements on π^+ production from carbon at 90° to the proton beam.

The cross-section determinations that are discussed have been made with nuclear emulsions. It is well known that many of the π^- mesons are brought to rest in the emulsion without producing observable disintegrations.[16] A very significant factor, which will affect the true value of any π^+/π^- ratio as well as the π^- production cross section, is an accurate knowledge of the number of "starless" π^- mesons that stop in the emulsion. Some earlier experiments determining the fractional contribution of "starless" π^- mesons have been reported.[17] These are reanalyzed and compared with more recent data.

II. GENERAL DESCRIPTION OF THE EXPERIMENT

Two different methods were employed for the measurement of positive and negative production cross sections at 0° and 90° to the proton beam. A uniform magnetic field was used for the study of $\pi^{\pm}$ cross sections at 0° and π^{+} cross sections at 90°. In this case the target dimensions perpendicular to the direction of the proton beam were large in comparison with the cross sectional area of the beam. Thus the conditions of infinite target and finite beam were easily approximated and the cross section was determined by the relation

$$\frac{d^2\sigma(T_\pi, \theta)}{dT_\pi\, d\Omega} = C_1 \frac{N_\pi(T_\pi, \theta)}{N_p \rho_t} \quad , \tag{1}$$

where C_1 is a measurable geometric factor, $N_\pi(T_\pi, \theta)$ is the number of pions per cm^2 per Mev that are incident on the front face of the absorber containing nuclear emulsion, N_p is the total number of protons that have passed through the target, and ρ_t is the number of carbon nuclei per cm^2. The π^+/π^- ratios at 0° to the proton beam are determined by first obtaining both the positive and negative pion production cross sections and then dividing one of these by the other.

The π^- production cross sections and the π^+/π^- ratios at 90° to the proton beam are obtained by using a heterogeneous magnetic field shaped to conform with the spiral-orbit principle. This principle is based on the fact that a charged particle describes a spiral orbit if it starts radially from the central axis of a heterogeneous magnetic field that is axially symmetric and decreases gradually as the radius increases. When a certain relationship between the field strength and the momentum of the particle is fulfilled, the orbit converges to a definite circle. For these 90° studies the conditons of infinite beam and finite target were approximated by keeping the target dimensions (perpendicular to the direction of the beam) smaller than the cross-sectional area of the beam. Thus the cross section for pion production can be determined from the relation

$$\frac{d^2\sigma(T_\pi, \theta)}{dT_\pi\, d\Omega} = C_2 \frac{q_\pi(T_\pi, \theta)}{I_p N_t} \quad , \tag{2}$$

where C_2 is an empirical geometric factor, $q_\pi(T_\pi,\theta)$ is the observed pion density in the nuclear emulsion, I_p is the total number of protons per cm^2 incident on the target, and N_t is the total number of nuclei comprising the target.

One of the purposes of this study is to determine empirically the behavior of the geometric factor, C_2. Once this geometric factor is accurately known, the π^--production cross sections for carbon, or for that matter, the $\pi^\pm$ cross sections for any element, can easily be determined by using Eq. (2). It has been shown[13] that for the measurement of any π^+/π^- ratio by the spiral-orbit principle only a knowledge of q_π is necessary. It was in this way that the π^+/π^- ratios from carbon at 90° to the proton beam were obtained. As a result two alternative ways were available for obtaining the cross sections for π^- production at 90° to the beam. One of these was to determine the behavior of C_2 and use Eq. (2). The second method was by direct calculation from the accurately determined π^-/π^+ ratio and the cross section for π^+ production. The second of these two methods was used because at this time it yielded the more accurate results.

III. DETAILS OF EXPERIMENTAL PROCEDURE

A. Proton Source and Collimation

For these studies the electrically deflected proton beam[18] from the 184-inch synchrocyclotron was used. In principle, the mechanism for producing the deflected beam is shown in Fig. 1a. As illustrated, a portion of the full-energy circulating proton beam enters a 120° sector of an electric deflector. The radius of the deflector at the beam entrance is approximately 81-1/4 inches and at the beam exit about 77 inches. A pulsed voltage of approximately 200 kilovolts, having a 0.1-microsecond rise (from 10 percent to 90 percent of full voltage) and a duration of 0.2 microseconds, is applied by a pulse transformer. This action causes an inward motion of the proton, resulting in a displacement of its orbit. This displacement of the orbit permits a certain fraction of the beam to enter the channel of the magnetic deflector. The magnetic deflector is in reality a magnetic shunt. Thus the strength of the magnetic field within this channel is reduced without disturbing the orbits that have not undergone displacement. This reduction in field strength causes a large increase in the radius of the proton path, resulting in deflection of the proton into an 8-inch-diameter evacuated tube leading to the experimental "cave". A focusing magnet about 7 feet from the vacuum chamber bends the beam through 18° so as to direct it to the cave, and also brings it to a horizontal focus approximately 24 feet from the magnet in the cave. Either a pair magnet or a 22-inch spiral-orbit spectrometer was placed here. The final beam dimensions, determined by the 48-inch snout collimator, were adjusted accordingly.

B. Experimental Studies with Uniform Magnetic Field (Pair Magnet)

1. Detailed Description of Experimental Method

It has been shown[19] that with this external proton beam a very simple method can be used for measuring absolute cross sections for pion production from any element. This in turn was modified[20] to permit the studies of these cross sections at any angle to the proton beam. The method has been standardized[1] so that the comparison of the measured cross sections at different angles, from different elements and by different experimenters, was simplified. The changes

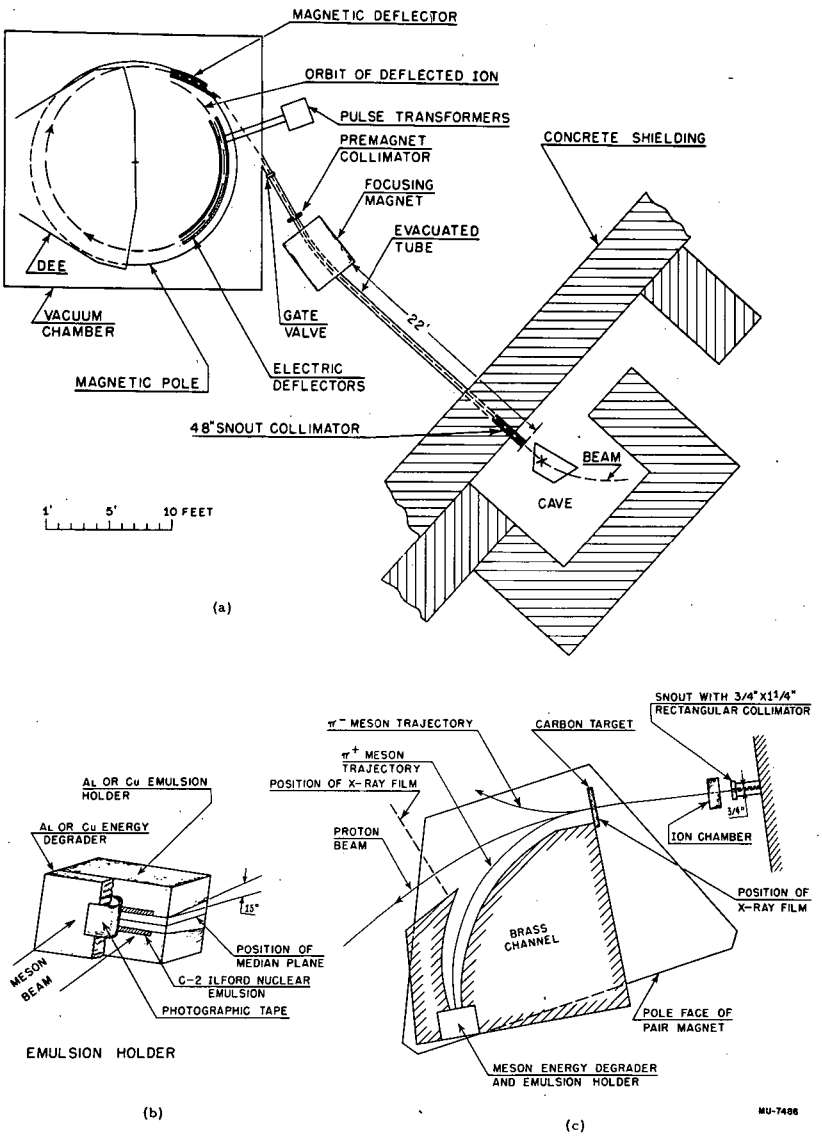

Fig. 1. Schematic of
(a) 340-Mev proton source,
(b) poor-geometry pion detector, and
(c) poor-geometry experimental arrangement.

that were introduced consisted of a more flexible pole tip and method of alignment of the proton beam.

Figure 1 c illustrates schematically the experimental arrangement. The proton beam was collimated by a 48-inch rectangular collimator having cross-sectional dimensions of 1-1/4 inches vertically and 3/4 inch horizontally. The collimated beam passed through an accurately calibrated (argon-filled) ionization chamber (Appendix), which measured N_p, the number of protons incident on the target. The beam then traversed the carbon target, which was placed in a uniform magnetic field. Positive and negative pions produced by the interaction of protons with carbon nuclei in the forward direction were magnetically separated from the proton beam. Of these created pions, only those of small energy and small angular intervals were selected by brass channels; they were magnetically bent through approximately 90°. These pions were incident normal to the front face of either an aluminum or a copper absorber, which contained nuclear emulsions (Fig. 1 b). The pions were stopped through their ionization loss in the absorber, and the incident number $N_{\pi}(T_{\pi}, \theta)$, was determined for each energy region by the measured pion density, $q_{\pi}(T_{\pi}, \theta)$, in the nuclear emulsion.

Except for the lowest pion energy, only one energy interval and one type of charged pion were investigated at one time. To measure the cross section for the pion of opposite charge in the same energy interval, the magnetic field was reversed by a reversing switch and the magnet was realigned. Furthermore, an additional channel section was added for the measurement of each negative cross section. This channel section was not used during the positive-cross-section measurement because it would extend into the proton beam. For the lowest pion energy the negative and positive cross sections were measured during the same exposure.

In no case was an exposure made before the alignment was better than 1/2 degree. This was accomplished by means of a template (1/8-inch brass or 1/4-inch plywood) for each channel energy, to which the channel sections were fitted. Proton and pion trajectories were accurately scribed on this template. Two film holders, which were aligned and firmly fixed to the template, contained pierced unexposed x-ray film defining the desired center of the proton beam (Fig. 1 c).

In addition, each film holder contained a small arrow-shaped proton absorber located at the desired beam positon. Two-second exposures were taken at low beam level, yielding light x-ray-film exposures. Any misalignment was easily determined by measuring the distance between the x-ray-film holders and the images of the two arrow absorbers appearing on the second x-ray film.

The study of the 90° spectrum of π^{+} production followed the same basic principle. For these measurements the face of the carbon target was placed at an angle of 45° to the direction of the beam, while the channel was so set that the mean pion trajectory (defined by the channel) left the target at 90° to the direction of the beam. In this case three x-ray pictures, one of which was located at the target position, were taken for the purpose of alignment.

2. Magnetic Field and Channel

The magnetic field that separated the pion and proton trajectories and deflected the pions into the detector had a maximum field strength of 14.4 kilogauss across a 3.4-inch gap. The area of the face (Fig. 1c) was large enough to permit a deflection of 70° for a 160-Mev pion in a uniform field (2% variation) at a 14.0-kilogauss setting. The magnetization curve (from 5.6 kilogauss to maximum field strength) at the center of the pole face was obtained with a proton magnetic resonance method. Field uniformity measurements were made with a flip coil, which had previously been calibrated by the proton magnetic resonance method. Furthermore, a magnetization curve (from 7.0 kilogauss to maximum field strength) was obtained with a flip coil at approximately 3-1/2 inches from each of the four edges of the pole face. The departure from uniformity increased with field strength to a maximum variation of 2.2% at maximum field between the center and the 3-1/2-inch position of the three pole-face edges. The channel was positioned in such a way as to take full advantage of the uniform field.

Five different channels for covering the 0° pion spectra and four channels for the 90° π^{+} spectrum were used. The channels have several purposes. They serve as shields for the detectors by preventing particles that leave the target at angles other than 0° from reaching the emulsion. Furthermore they permit only those protons to reach the absorbers that have the same momentum range as the pions. For all

channels this proton momentum range is below the threshold for pion production in the absorbers containing the emulsions. As a result the largest source of pion contamination is eliminated. Contaminating pions are also produced by protons that are scattered from the target into the pole faces of the magnet. Because of the critical channel requirements this source of pion contamination is greatly minimized. For the calculation of the cross sections this contamination was considered negligible, because no negative pions were found in the π^+ plates and only five positive pions were observed in the entire volume of emulsion used for the measurement of the π^- cross sections at 0°.

The minimum width of the channel, which is fixed by the requirements of "poor geometry", defines the angular acceptance of the detector. For the π^+ spectrum at 0° the accepted half angular spread was 2.5°, whereas for the π^- spectrum, and the π^+ spectrum at 90°, the accepted half angular spread was 2°. This minimum width likewise provides a selection of the energy interval by accepting only those pion trajectories with the correct curvature. In all cases this energy interval was broader than the energy interval of the scanned emulsion.

A mean lateral displacement of the pion from its original trajectory is introduced through multiple Coulomb scattering, which it undergoes when the pion energy is degraded in the absorber. The desired condition of poor geometry is that the cross-sectional dimensions of the absorber on which the pions are incident, and therefore the dimensions of the minimum width of the channel, be large compared with this lateral displacement. Thus the necessary condition of poor geometry--that as many pions have scattered into that part of the pion beam which stops in the scanned region of emulsion as have scattered out of it--can be assumed as fulfilled.

Two methods were considered for calculating this lateral displacement. One of these consisted of using the modified[21] Fermi distribution functions for the lateral and angular displacement of charged particles that undergo multiple elastic scattering in passing through matter. These distribution functions were generalized to take into account, to a good approximation, the energy loss of the charged particle along its scattered trajectory. The second method was to use the approximate but simple relation,[22] $y_{rms} = 0.03\, R\sqrt{Z}$, where R is the calculated range of the pion in an absorber whose atomic number is Z.

The two methods yield different results. A plot of the lateral displacements from the two methods against pion energy shows a crossover at a pion energy of 30 Mev. The resulting values continue to diverge with increasing pion energy so that for a 110-Mev pion the simple relation reports a lateral displacement three times as large as that which is obtained from the modified Fermi functions. To insure that the poor-geometry conditions were met, the channel was designed in such a way that the total minimum width was about 7 y_{rms}, where for y_{rms} the larger value obtained from the two methods was chosen.

For such a geometry it has been shown[23] that the solid angle subtended at the target by a unit area at the emulsion which is perpendicular to the undisturbed trajectory of the pion is given by

$$\frac{d\Omega}{dA} = \frac{1}{\rho^2 \phi \sin \phi} = \frac{1}{C_1} \quad , \tag{3}$$

where ρ is the radius of curvature of the mean pion trajectory in the channel and ϕ is the angular distance between the center of the target and the center of the planned scanning region in the absorber. This relation was obtained by considering that the trajectories lie in a plane perpendicular to the uniform magnetic field. A small error is introduced by the use of this formula for pions whose trajectories have a small component along the direction of the magnetic field. Since the target and the sensitive area of the emulsion were finite in size, this condition did exist. For the dimensions used in this experiment, however, this error was less than 0.1 percent.

3. Targets

The effective area of the carbon targets was defined by the collimated proton beam. The targets varied from 0.511 g/cm^2 for the lowest pion energy to 1.540 g/cm^2 for the highest energy, and each was of uniform thickness. The thickness of the target introduces three undesirable factors into the experimental results:

(a) The proton energy loss in the target increases with thickness. If this proton energy loss becomes appreciable, a correction to the measured cross section that is obtainable from the excitation function for pion production becomes necessary.

(b) The thickness affects the pion-energy resolution for the measured cross section, because pions emerging from the target with

that energy interval that is selected by the channel are produced at different depths in the target. Hence we cannot surely know at what energy these pions are created, because as the pions pass through the target to the point of emergence, variable amounts of their original energy are lost.

(c) A thick-target correction resulting from this random position of pion creation must be applied to the measured cross section. The magnitude of this correction increases with target thickness.

In choosing the thickness of the target for each measurement of the cross section a compromise was made between these factors and the tolerable pion-to-background ratio in the emulsion.

The volume of each target was obtained from its dimensions, which were obtained by micrometer measurements. The densities of the targets were calculated from the measured weights and volumes. From these measurements the number of carbon nuclei per cm^2, ρ_t, in each target was determined by the relation

$$\rho_t = Dt \frac{A_o}{A} \qquad (4)$$

where D, t and A are respectively the density, thickness and atomic number of the target, and A_o is Avogadro's number.

4. Pion Detection

The nuclear-emulsion technique used as the mode of pion detection consisted of studying the endings of the stopped particles in Ilford C-2 200-micron nuclear emulsions. The positive pions were identified by their characteristic π-μ-decay endings, while most of the negative pions were identified by the star that results from the disruption of the nucleus following nuclear capture of the pion. A great aid for this method of detection was the choice of the angle α at which the emulsion was inclined to the median plane of the magnetic field. It was 15^o, therefore most of the pions entered the surface of the emulsion at small angles, and as a result were easily distinguished from the background through their characteristic scattering and the rapid change of grain density as the pions approached the ends of their ranges. These were the criteria used for distinguishing starless negative pions from protons having the same residual range.

To stop the incident pions, the nuclear emulsions were imbedded in aluminum absorbers for pion energies below 60 Mev and in copper absorbers for larger pion energies. The emulsion holders held the leading edge of the emulsion 0.3 inch from the median plane of the magnetic field. For each cross-section measurement three different exposures were obtained in one run; the lower holder was kept in place throughout the exposure period, while the upper holder was replaced by another one part way through the exposure. That emulsion found, on development, to have the most favorable pion-to-background ratio was used for the measurement of the cross section.

The total number of pions of energy T_i incident per unit area on the face of the detector, in a given energy interval ΔT, is $N(T_i)\Delta T$; these can be related to the density of pions in the emulsion, $q(T_i)$. For simplicity in Fig. 2 the approximation is made that the pion paths in the absorber are straight lines. These trajectories are not straight, however, (see below), and the following relations are not dependent on this approximation.

Consider an element of volume of the emulsion whose true thickness is d (Fig. 2). The number of pions in the energy interval ΔT that stop in the emulsion is given as n, which is equal to $N(T_i)\Delta T\Delta A$, where ΔA is an element of area perpendicular to the pion path at the emulsion. This element of area could be the area $a \cdot \ell$ where ℓ is the scanning distance, perpendicular to the plane of Fig. 2. The energy of an observed pion can be expressed in terms of its true range R, i.e.,

$$T = T(R) = T\left\{M_1 + R'\left[T'(x)\right]\right\} \quad .$$

M_1 is the length of the pion path in the absorber before entering the surface of the emulsion, and x is the length of that part of the path that lies in the emulsion. $T'(x)$ is the energy of the pion of range x in the emulsion; $R'(T')$ is the range of the pion of energy T' in the absorber. From this expression we can obtain a relation between the pion energy interval ΔT, which corresponds to the effective thickness of the emulsion $d \csc \alpha$. Thus

$$\Delta T = \frac{dT}{dR}\frac{dR}{dx}\Delta x = \frac{dT}{dR}\frac{dR}{dR'}\frac{dR'}{dT'}\frac{dT'}{dx}\Delta x \quad ;$$

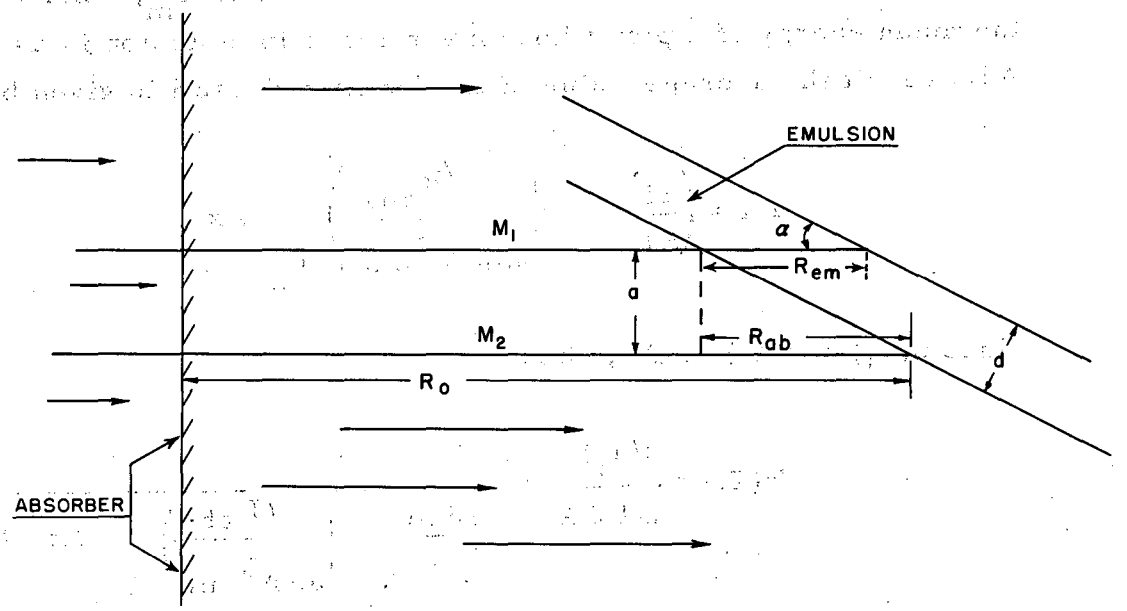

Fig. 2. Diagram symbolizing relation between pion flux and pion density in the emulsion.

$$\Delta T = \left(\frac{dT}{dR}\right)_{T_i} \Big|_{abs} \left\{ \frac{\left(\frac{dT}{dR}\right)_{abs}}{\left(\frac{dT}{dR}\right)_{em}} \right\}_{T'} \Delta x \quad ; \qquad (5)$$

since $\frac{dR}{dR'} = 1$,

where subscripts abs and em refer respectively to measurements of these quantities in absorber and emulsion, while T_i, as previously, refers to the mean pion energy as determined by the channel. Equation (5) must be averaged over all possible values of T'. For the case where $\Delta x = d \cdot \csc \alpha$ these values of T' vary from zero to T_m, where T_m is the mean energy of a pion whose mean range in emulsion is $d \cdot \csc \alpha$. As a result the average value of ΔT for $\Delta x = d \cdot \csc \alpha$ is given by

$$\Delta T = \left(\frac{dT}{dR}\right)_{T_i} \Big|_{abs} \left(\frac{R_{abs}}{R_{em}}\right)_{T_m} \Delta x \quad .$$

Since $n(T_i) = N(T_i)\, \Delta T\, \Delta A$, then

$$N(T_i) = \frac{n(T_i)}{\Delta T\, \Delta A} = \frac{n}{\left(\frac{dT}{dR}\right)_{T_i} \Big|_{abs} \left(\frac{R_{abs}}{R_{em}}\right)_{T_m} \Delta x\, \Delta A} =$$

$$\frac{q(T_i)}{\left(\frac{dT}{dR}\right)_{T_i} \Big|_{abs} \left(\frac{R_{abs}}{R_{em}}\right)_{T_m}} \qquad (6)$$

This is the desired relation between (a) the total number of pions of energy T_i per cm^2 per Mev that are incident on the face of the absorber and (b) the density of these pions at this energy in the emulsion. For these experiments the following values for $\left(\frac{R_{abs}}{R_{em}}\right)$ were used: for copper 0.420; for aluminum 1.165. As shown in Fig. 18b, where the calculated values of these ratios are plotted against pion energy,

only a 2.6% variation is expected in this ratio for pion energies from 2 Mev to 9 Mev. The value for the energy T_m should lie within this energy interval.

The number of pions that had stopped in the emulsion was determined with a microscope using a 97x oil-immersion objective and 6x eye pieces. This microscope was equipped with a special stage that enabled the observer to reset the microscope with an accuracy of about 2 microns. With this arrangement the scanned area was accurately measured. For all these experiments the emulsions were scanned by the same observer. A series of checks was made on the scanning efficiency during this period by (a) rescanning by the original observer of areas selected at random, (b) rescanning by new scanners of areas selected at random. For this second method a total of 385 π^+-mesons was found by new scanners having an estimated efficiency of 85%. In this total number not one meson was found that had not been recorded previously. On the basis of these results, and also because of the favorable pion-to-background ratio, a scanning efficiency greater than 97% is assumed.

The thickness of the emulsion was measured in two ways: (a) A difference micrometer was used to measure the combined thickness of the glass and the emulsion immediately before exposure. For each plate the mean of 14 readings was taken. After the development, these same quantities were measured again, as well as the glass thickness alone, for each plate. To permit direct measurement of the glass a 1/4-inch region of the emulsion was completely removed from each end of each plate. (b) A microscope with a calibrated rack was used to measure the thickness of the emulsion at the scanning region. The measured shrinkage factor was applied to this value to give the true thickness of the undeveloped emulsion. An average of the measurements by micrometer and by microscope was taken whenever there was a discrepancy of 2% between the two measurements. Otherwise the value obtained from the micrometer measurement of the emulsion thickness was used.

The energy T_i of the pion incident on the face of the detector was obtained from the relation between its momentum, its mean radius in the channel, and the strength of the magnetic field. The value of this

energy was converted to the mean range of the pion in the absorber by modifying, in the conventional manner, the range-energy tables[24] calculated for protons. The actual position in the absorber of this calculated range (which determines the position of the scanning area) is influenced by several factors that affect the energy of the pion upon its passage through matter. These are: (a) small-energy-transfer inelastic events, (b) the variation of the nuclear absorption and large-angle scattering cross section with energy, (c) elapsed flight time of the pion, (d) energy distribution of the incident beam, (e) range straggling, and (f) multiple Coulomb scattering. The first three have but a minor effect on the range shortening. They are, however, considered as corrections to the measured cross section. The last two factors must be considered in detail, for they may have a considerable effect on pion range shortening, particularly in the low-energy region.

An illustration of this range shortening for monoenergetic proton and pion beams is presented in Fig. 27 and Fig. 14b. Figure 27 is a plot of the region near the end of the projected range in copper for a 340-Mev proton beam. As explained later, this is not an integral range curve. As the calculated range in copper for a 340-Mev proton is 92.7 g/cm^2, the possible range shortening in this case is estimated at 3%.

Figure 14b is a plot of a portion of the projected range-straggling curve for 9.2-Mev pions in aluminum. In this case the peak of the pion distribution may have shifted to 69% of the actual calculated range. This estimate may in part be substantiated by the projected range curve for a monoenergetic 8-Mev beam of pions in emulsion,[25] where the peak of the observed pions occurs at approximately 68% of the calculated range. Such large differences between the calculated range and the projected range at which the maximum pion distribution occurs is not expected for high-energy pions. However, account must be taken of this gradual fall-off of the integral range curve for pions, since the location of the correct scanning area is vital to the success of this detection technique. It is obvious that an erroneous choice could not only seriously influence the apparent shape of the observed spectrum but also alter the over-all magnitude of the total cross section.

For the study of a slowly varying continuous spectrum, this problem of proper location of the scanning region is greatly simplified.

Since the channel is designed to accept pions of a definite energy distribution, it may be assumed that the pion distribution in the absorber as a function of projected range is Gaussian for each energy within this interval. A fold of these Gaussian distributions for all the accepted energies produces a sizable flat distribution of pions in the absorber about the position of the projected range for a pion whose mean energy is defined by the channel. The probable position of this projected range was obtained by calculating the range shortening resulting from multiple scattering and range straggling by the previously reported methods.[23, 1]

The scanning area was chosen in such a way that when these considerations were taken into account, the accepted half angular spread about the mean angle of observation corresponded to the previously mentioned values. For all but the lowest energy, the scanning interval corresponded to an energy spread that was appreciably smaller than that introduced by the target. For these cross sections the energy half width of the production target was taken as a good approximation for the energy resolution. For the lowest-energy cross sections the reverse situation existed, and therefore the energy half width of the scanning area was used for the energy resolution.

5. Calculation of the Cross Section

By combining equations 1, 3, 4, and 6 one arrives at the expression for the differential cross section,

$$\frac{d^2\sigma\,(T_i, \theta\,)}{dT\,d\Omega} = \frac{q(T_i, \theta)}{\left(-\frac{dT}{dR}\right)_{T_i}\Big|_{abs}\left(\frac{R_{abs}}{R_{em}}\right)_{T_m} N_p\,Dt\left(\frac{A_o}{A}\right)\left(\frac{d\Omega}{dA}\right)}$$

(in units $cm^2 Mev^{-1} steradian^{-1} nucleus^{-1}$), which was used to calculate the results presented. Three corrections were applied to this calculated cross section.

a. Correction for pion decay in flight

Because of the unstable nature of pions, some of those pions created in the target decay before reaching the emulsion. The relative probability that a positive or negative pion of mean life[26, 27] $\tau_\pi = 2.54 \times 10^{-8}$ sec survives a time $\tau(T_i)$ in its proper frame is

$\exp-(\tau/\tau_\pi)$. The value of $\tau(T_i)$ was obtained by integrating

$$d\tau = dt\sqrt{1 - v^2/c^2} = \frac{m_\pi c^2}{p_i c^2}\, ds$$

over the entire pion trajectory. Here dt represents the corresponding time in the laboratory frame of reference; v, m_π, and p_i are respectively the velocity, rest mass and momentum of the pion; ds is the element of the path length traveled in time dt; and c is the velocity of light. The elapsed proper time during the pion's flight in air, τ_{air}, is easily calculable, as the change in pion momentum is negligible in air. This time is given by,

$$\tau_{air} = \frac{m_\pi c^2}{p_i c^2}\,\rho\phi' = 3.3 \times 10^{-11}\left(\frac{m_\pi c^2}{2T_i}\right)^{\frac{1}{2}}\left(1 + \frac{T_i}{2m_\pi c^2}\right)^{-\frac{1}{2}}\rho\phi' =$$

$$1.565 \times 10^{-5}\,\frac{\phi'}{H} \quad \text{seconds},$$

where ρ is the mean radius of the channel, and ϕ' (expressed in radians) is the angle through which the trajectory of a pion of energy T_i (Mev) is bent in air by a uniform magnetic field of strength H (gauss).

To compute the elapsed proper time τ_{abs} in absorber, two approximations were made: (1) the pion momentum in the absorber is given by the nonrelativistic approximation $p_\pi^2 = 2mT_\pi$; (2) the empirical range-energy relation[28], $T_\pi = KR^{0.58}$ where K is a constant of the absorber, can be used. As the time spent by the pion in absorber is approximately 10% of its time in air, the errors introduced by these approximations can be neglected. Then

$$\tau_{abs} = \int \frac{m_\pi}{p_\pi}\, ds = \frac{m_\pi}{2\sqrt{K}} \int_0^R \frac{dR}{R^{0.29}} = 4.70 \times 10^{-11}\left(\frac{m_\pi c^2}{2T_i}\right)^{\frac{1}{2}} R \text{ sec.},$$

where R is the range in centimeters of absorber. The total lapsed time $\tau(T_i) = \tau_{air} + \tau_{abs}$ and therefore the calculated cross section was multiplied by $\exp\left[10^8\tau(T_i)/2.54\right]$.

b. Correction for thick target

The quantity measured in the experiment is the number of pions of energy T emerging from the target in an energy interval ΔT that

is defined by the channel. These pions have been produced at various depths in the target with energies $T' = T + \left(\frac{dT}{dx}\right)_{T'} \delta x$, where δx is the mean target thickness between the point of pion creation and its point of exit from the target. Therefore a relation must be obtained between the energy interval at production $\Delta T'$ and the observed energy interval ΔT. We may express the pion energy at production as a function of its mean range R in the target material by $T' = T'(R) = T' \left[\delta x + R_E(T)\right]$ where $R_E(T)$ is the mean range in the target material of a pion with exit energy T. As this expression is a function of T and δx, we can differentiate with respect to T while holding δx constant to obtain the relation

$$\Delta T = \frac{\left(\frac{dT}{dR}\right)_T}{\left(\frac{dT}{dR}\right)_{T'}} \Delta T' \quad . \tag{8}$$

Since this result holds for any fixed δx, it must be averaged over the range of the possible δx values. The values of δx vary from zero to t as T' changes from T to $T + \delta T$, where δT is the mean energy loss through the target of thickness t of a pion that was created at the front face of the target and emerged with an energy T. An average of Eq. (8) over the range of δx for a fixed energy T gives

$$\frac{\Delta T}{\Delta T'} = \left(\frac{dT}{dR}\right)_T \frac{t}{\delta T} \quad .$$

The calculated cross sections are multiplied by this factor and are reported as though the pions originated at the center of the target.

c. Correction for nuclear interaction and large-angle scattering in the absorber

As previously stated, some of the pions incident on the absorber are removed from the pion flux at the emulsion by nuclear absorption and large-angle scattering during the slowing-down process in the absorber. The available experimental data[29, 30] for such nuclear interactions on various materials and at several energies are mainly in the form of total cross sections, and are not too reliably separated into contributions due to inelastic scattering, to nuclear absorption, and to large-angle elastic scattering. To make an accurate correction for these effects one needs information on the energy dependence

of these components of nuclear interaction. As this is not available, an approximate correction to the cross-section calculations can be made, since the experimental information on these effects suggests that the assumption of geometric nuclear area πr^2 for the total nuclear attenuation cross section σ_a may be satisfactory. Therefore each calculated cross section was multiplied by $\exp(\mu\rho t)$ where $\mu = \sigma_a A_o/A$, A_o is Avogadro's number, ρt is the thickness of the absorber in grams per cm^2, $r = 1.4 \times 10^{-13} A^{1/3}$ cm, and A is the atomic weight of the absorber.

6. Experimental Results

All experimental results are presented in tabulated and plotted form.

a. Positive-pion cross sections

1. Table I contains the data obtained for production of positive pions from carbon at 0° to the proton beam. It is based on 1281 pion events. The following notation is used. The expression $\left(\frac{d^2\sigma^+}{dTd\Omega}\right)_{uncorr}$ represents the calculated differential production cross section in units of $cm^2 Mev^{-1} steradian^{-1} nucleus^{-1}$ for energies of pions that are created at the center of the target, as it is obtained from Eq. (7). The expression $\left(\frac{d^2\sigma^+}{dTd\Omega}\right)_{a,b}$ is the value of $\left(\frac{d^2\sigma^+}{dTd\Omega}\right)_{uncorr}$ after it has been corrected for (a) pion decay in flight, and (b) thick target. Likewise $\left(\frac{d^2\sigma^+}{dTd\Omega}\right)_{a,b,c}$ is the value of $\left(\frac{d^2\sigma^+}{dTd\Omega}\right)_{uncorr}$ when corrected for (a) pion decay in flight, (b) thick target, and (c) nuclear interaction and large-angle scattering in the absorber. A plot of $\left(\frac{d^2\sigma^+}{dTd\Omega}\right)_{a,b}$ and $\left(\frac{d^2\sigma^+}{dTd\Omega}\right)_{a,b,c}$ as a function of pion energy is presented in Fig. 3. On this figure the probable shapes of the experimental spectra are sketched in for these two cases. The area under the curve for $\left(\frac{d^2\sigma^+}{dTd\Omega}\right)_{a,b,c}$ was obtained by means of a histogram. This value appears in Table I. The errors given are probable errors of purely statistical origin.

Table I

Cross Sections for Positive-Pion-Production from Carbon at 0° to a 340-Mev Proton Beam

T_π (Mev)	n_π No. of pions	$\left(\frac{d^2\sigma^+}{dTd\Omega}\right)_{uncorr} \times 10^{30}$ $\frac{cm^2}{Mev\text{-}Ster\text{-}Nucleus}$	Corrections (a) Time of flight	(b) Thick target	(c) Nuclear interaction	$\left(\frac{d^2\sigma^+}{dTd\Omega}\right)_{a,b} \times 10^{30}$ $\frac{cm^2}{Mev\text{-}Ster\text{-}Nucleus}$	$\left(\frac{d^2\sigma^+}{dTd\Omega}\right)_{a,b,c} \times 10^{30}$ $\frac{cm^2}{Mev\text{-}Ster\text{-}Nucleus}$
15.7	79	3.63 ± 0.28	1.15	1.06	1.02	4.24 ± 0.34	4.49 ± 0.34
37	153	6.15 ± 0.34	1.10	1.04	1.08	7.00 ± 0.38	7.56 ± 0.41
56	173	9.20 ± 0.47	1.09	1.03	1.18	10.34 ± 0.53	12.16 ± 0.62
72	284	11.62 ± 0.46	1.08	1.02	1.23	12.73 ± 0.51	15.72 ± 0.63
90	242	14.16 ± 0.61	1.08	1.01	1.35	15.42 ± 0.67	20.76 ± 0.90
112	202	10.69 ± 0.50	1.07	1.00	1.52	11.46 ± 0.54	17.38 ± 0.82
132	123	8.97 ± 0.54	1.06	1.00	1.70	9.55 ± 0.58	16.19 ± 0.98
162	25	3.01 ± 0.40	1.06	1.00	2.04	3.18 ± 0.43	6.48 ± 0.87

Based on 1281 Pions $\left(\frac{d\sigma^+}{d\Omega}\right)_{a,b,c} = (21.04 \pm 0.50) \times 10^{-28} \frac{cm^2}{Ster\text{-}Nucleus}$

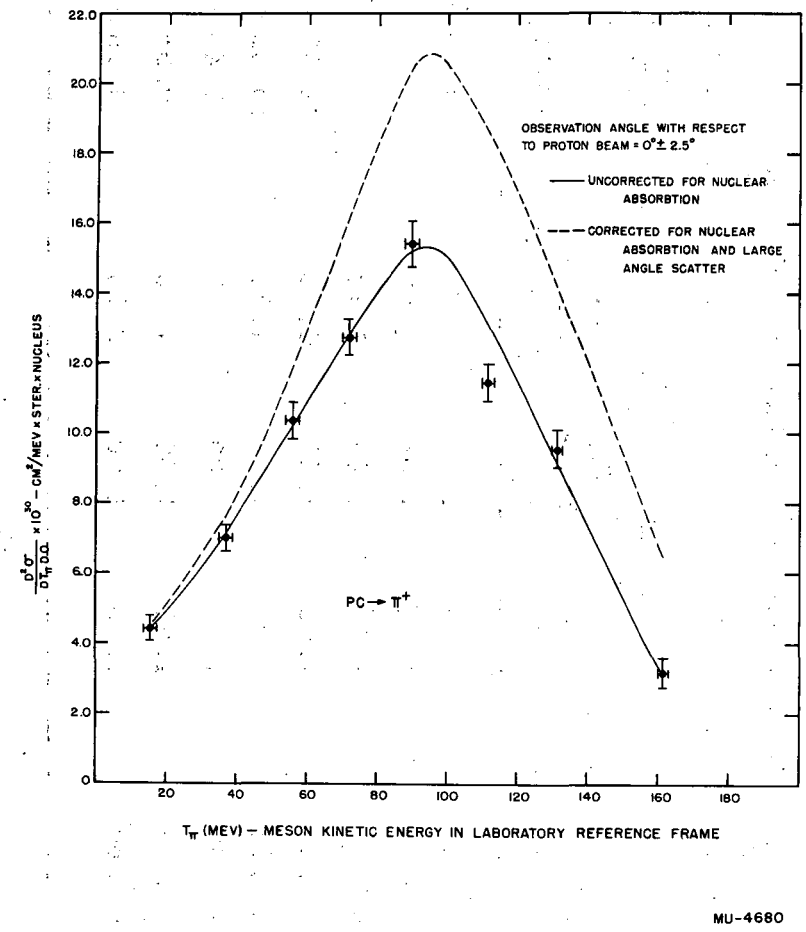

Fig. 3. Spectrum of production cross section for positive-pion production in carbon by 340-Mev protons.

2. Table II contains the results that were obtained for positive-pion production from carbon at 90° to the proton beam. These data are based on 1071 π-μ-decays. In presenting these results the same notation is followed as in Table I. Plots of $\left(\frac{d^2\sigma^+}{dTd\Omega}\right)_{a,b}$ and $\left(\frac{d^2\sigma^+}{dTd\Omega}\right)_{a,b,c}$ as a function of pion energy are presented in Fig. 4. The probable shapes of the experimental spectra are sketched in for the two cases. The area under the curve for $\left(\frac{d^2\sigma^+}{dTd\Omega}\right)_{a,b,c}$ was obtained by means of a histogram. This integral value appears in Table II. The errors given are probable errors.

b. Cross sections for negative pions

1. Prong distribution

It is a well-established fact that slow negative pions interact strongly with complex nuclei, and that these pions, if brought to rest in the emulsion, frequently produce observable nuclear disintegrations. It is also well known that some negative pions, when brought to rest in emulsion, produce no observable events. The requirement of Eq. (7) for π^- cross-section calculation is an accurate knowledge of the total number of negative pions that stop in a given volume of emulsion. Because the production cross sections from proton bombardment are usually much smaller for negative pions than for positive pions, much longer exposures are necessary if a significant number of negative pions are to be observed. As longer exposures introduce a larger background in the emulsion, it becomes progressively more difficult to identify the starless negative pion endings. The accepted procedure for measuring a π^--production cross section is to determine the number of star-forming negative pions in a given volume of emulsion. Therefore, in addition to the three corrections that were applied to Eq. (7) for the calculation of the π^+ cross section, another correction must be introduced for the calculation of the π^- cross section. This can be considered either as a correction for the detection efficiency of an observer using the emulsion technique for observing negative pions, or as a zero-prong correction. So as to minimize the over-all systematic error, it is important to analyze this correction factor.

Table II

Cross Sections for Positive-Pion-Production from Carbon at 90^{o} to a 340-Mev Proton Beam

T_π (Mev)	n_π No. of pions	$\left(\frac{d^2\sigma^+}{dTd\Omega}\right)_{uncorr} \times 10^{30}$ $\frac{cm^2}{Mev\text{-}Ster\text{-}Nucleus}$	Corrections (a) Time of flight	(b) Thick target	(c) Nuclear interaction	$\left(\frac{d^2\sigma^+}{dTd\Omega}\right)_{a,b} \times 10^{30}$ $\frac{cm^2}{Mev\text{-}Ster\text{-}Nucleus}$	$\left(\frac{d^2\sigma^+}{dTd\Omega}\right)_{a,b,c} \times 10^{30}$ $\frac{cm^2}{Mev\text{-}Ster\text{-}Nucleus}$
16.4	157	3.37 ± 0.18	1.17	1.09	1.02	4.31 ± 0.23	4.38 ± 0.24
37.5	395	4.12 ± 0.14	1.11	1.05	1.08	4.81 ± 0.16	5.19 ± 0.18
57	312	2.82 ± 0.11	1.09	1.04	1.18	3.19 ± 0.12	3.75 ± 0.14
73	133	1.87 ± 0.11	1.08	1.03	1.23	2.07 ± 0.12	2.55 ± 0.15
91	49	0.71 ± 0.07	1.07	1.02	1.35	0.77 ± 0.07	1.04 ± 0.10
112	25	0.41 ± 0.06	1.06	1.01	1.52	0.44 ± 0.06	0.67 ± 0.09

Based on 1071 Pions $\left(\frac{d\sigma^+}{d\Omega}\right)_{a,b,c} = (3.35 \pm 0.07) \times 10^{-28}$ $\frac{cm^2}{Ster\text{-}Nucleus}$

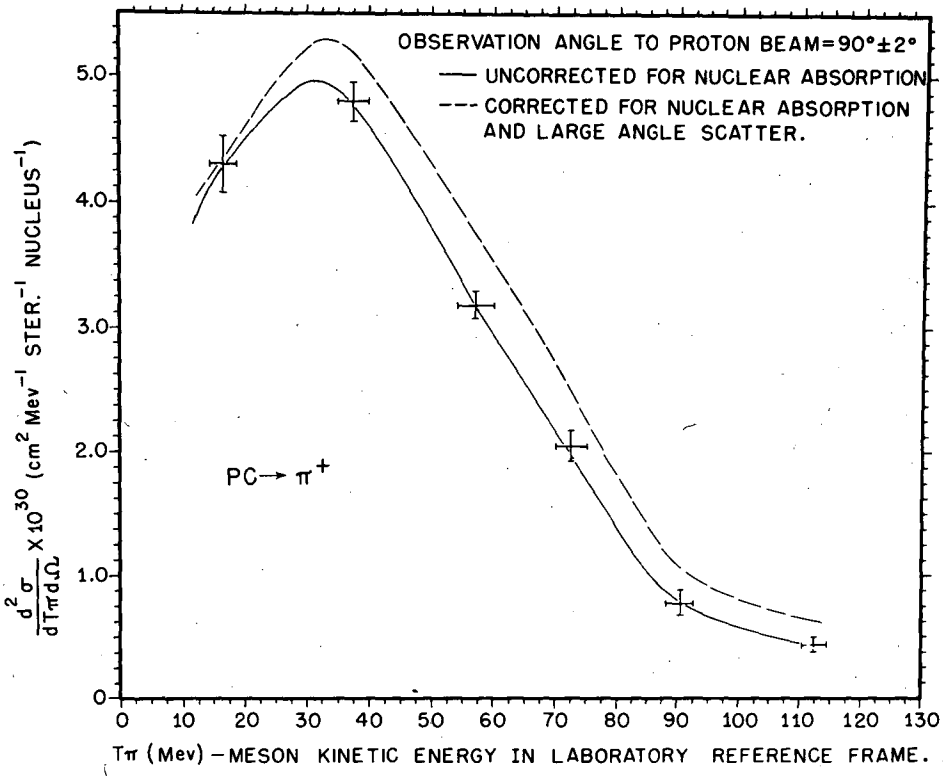

SPECTRUM OF PRODUCTION CROSS-SECTIONS FOR POSITIVE PIONS PRODUCED IN CARBON BY 340 Mev PROTONS.

Fig. 4.

Star prongs leaving the terminus of a negative pion have previously been studied in nuclear emulsions. The approximate numbers of stopped negative pions observed by different authors were: Perkins[31]--100; Adelman and Jones[17]--512; Cheston and Goldfarb[31]--500; Menon, Muirhead, and Rochat[17]--1800; and Adelman[31]--1631. The primary purpose of these observations, with the possible exception of those by Adelman and Jones, was to study the spectrum of fast protons arising from nuclear disintegrations that are caused by capture of negative pions. Furthermore, only two of these groups (Adelman and Jones, and Menon, Muirhead, and Rochet) have used the same convention as is used in these studies for defining a prong--any group of grains leaving the terminus of a pion with a well-defined direction is a star prong. The results obtained by these two groups are displayed in Table III, along with the prong distribution that was obtained from the production studies of the π^- spectrum at zero degrees to the proton beam.

The results of these three sets of data are in good agreement. In all cases where this zero-prong ratio was established, however, the emulsion contained a high proportion of background. Because of the nature of the exposure it is safe to assume that the nuclear plates obtained outside the cyclotron with the pair-magnet technique contained the largest pion-to-background ratio. From the scanning of these plates one can assume that the two groups of experimenters experienced at least the same amount of confusion in the interpretation of events that could be classed either as starless pions or background. Accordingly a star-prong distribution from π^- studies with Ilford C-2 emulsions using a spiral-orbit spectrometer was compiled; it is presented in Table III and Fig. 5 (a).

The spiral-orbit spectrometer plates in some cases contained a pion-to-background ratio that was at least 10^4 as large as in many of the nuclear plates obtained with the pair magnet. The emulsions exposed with the spiral-orbit spectrometer were remarkably clean of background tracks; in some instances an observer could locate 100 negative pions in the course of an eight-hour day. Although the use of the spiral-orbit spectrometer has greatly minimized the possibility of confusing starless pions with background, nevertheless, another difficulty has arisen. Because of the nature of the spiral-orbit principle,

Table III

Prong Distribution from Terminus of Stopped Negative Pions in Ilford Emulsions (In percent)

Experiment	How Exposed (No. of Events).	Number of prongs in star							
		0	1	2	3	4	5	6	7
Menon Muirhead Rochat	Inside 184" cyclotron (1137)	. . .	33.7 ± 1.7	33.1 ± 1.7	22.1 ± 1.4	9.3 ± 1.0	1.7 ± 0.4	0	0
	Cosmic radiation (665)	. . .	34.7 ± 2.3	28.1 ± 2.0	21.4 ± 1.8	13.5 ± 1.4	2.5 ± 0.6	0.3 ± 0.2	0
	Combined results	28 ± 2	24.4 ± 1.2	22.5 ± 0.9	15.7 ± 0.8	7.9 ± 0.6	1.4 ± 0.2	0.07 ± 0.07	0
Adelman Jones	Inside 184" cyclotron (512)	26.8 ± 2	21.5	27	15.2	7.8	1.8	0	0
Adelman	Inside 184" cyclotron (1631)	. . .	32.4 ± 1.0	32.7 ± 1.0	22.3 ± 0.8	10.5 ± 0.6	2.0 ± 0.2	0.1 ± 0.1	0
From 0° π^- Spectrum	Pair-magnet outside 184" cyclotron (853)	29.1 ± 1.8	27.9 ± 1.8	20.2 ± 1.5	15.8 ± 1.2	6.3 ± 0.9	0.6 ± 0.3	0	0.1 ± 0.1
90° Experiments on π^- Production	Spiral-orbit spectrometer outside 184" cyclotron (4882)	$\left(26.2\ ^{+0.3}_{-1.0}\right)$*	27.0 ± 0.7	22.6 ± 0.7	16.3 ± 0.6	6.9 ± 0.4	0.9 ± 0.1	0.16 ± 0.06	0.02 ± 0.02

* True Value is smaller. A small contamination correction is necessary.

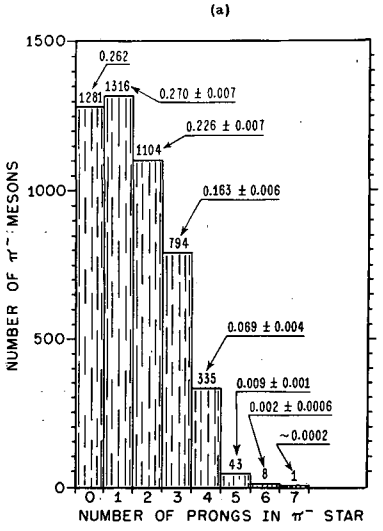

HISTOGRAM OF PRONG DISTRIBUTIONS
FOR 4882 π^- MESONS FROM
SPIRAL-ORBIT SPECTROMETER DATA.

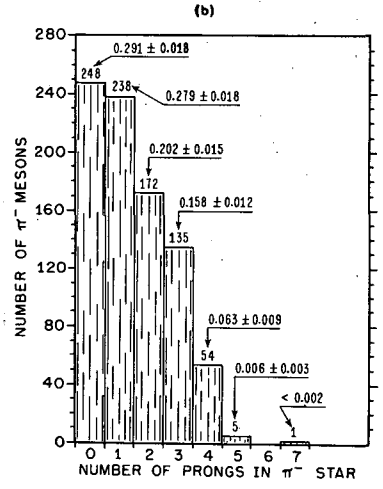

HISTOGRAM OF PRONG DISTRIBUTIONS
FOR 853 π^- MESONS
FROM FORWARD DIRECTION π^- DATA.

MU-7492

Fig. 5.

which is briefly discussed later, the determination of the possible μ^--meson contamination that is created during the flight time of some of the negative pions in the heterogeneous field becomes difficult. It is not easy to see that this contamination is very small. There is some direct experimental evidence, however, on the validity of this statement from the study of the "fly-back effect" in the measurement of the positron decay spectrum from μ^+ mesons.[32] These arguments are not considered in this paper. However, because of this μ^- contamination effect, one can say that the 26.2% appearing in Table III is an upper limit to the correction for starless negative pions. The negative error of this value has been increased in Table III to compensate for the possible μ^- contamination.

To summarize: Each π^- cross section was obtained by determining the number of star-forming negative pions and correcting this number by the factor 1.35 (i.e., taking account of a 26% zero-prong correction) to obtain the total number of negative pions that stopped in a given volume of emulsion.

2. π^- Spectrum at 0° to the proton beam

Table IV contains a summary of the results from the π^--production experiment on carbon at 0° to the proton beam. These data are based on 605 star-forming negative pions. The notations are the same as are used in Table I except for the fact that here $\left(\frac{d^2\sigma^-}{dT d\Omega}\right)_{uncorr}$ contains the zero-prong correction. A plot of $\left(\frac{d^2\sigma^-}{dT d\Omega}\right)_{a,b}$ and $\left(\frac{d^2\sigma^-}{dT d\Omega}\right)_{a,b,c}$ as a function of pion energy is presented in Fig. 6. The area under the curve for $\left(\frac{d^2\sigma^-}{dT d\Omega}\right)_{a,b,c}$ was determined by means of a histogram, and is presented in Table IV. As previously, the reported errors are probable errors of purely statistical origin.

c. Production ratios of charged pions at 0° to the proton beam

From the production cross sections for positive and negative pions at 0°, one can obtain either the π^+/π^- or the π^-/π^+ ratios. For convenience, both of these ratios and their probable errors were calculated for each pion energy and are presented in Table V and in Fig. 7. The value for the ratio of the integrated cross sections $\left(\frac{d\sigma}{d\Omega}\right)_{a,b,c}$ at 0° is given in Table V.

Table IV

Cross Sections for Negative-Pion Production from Carbon at 0° to a 340-Mev Proton Beam

T_π (Mev)	n_π^* No. of star-forming pions	$\left(\frac{d^2\sigma^-}{dTd\Omega}\right)_{uncorr} \times 10^{31}$ $\frac{cm^2}{Mev\text{-}Ster\text{-}Nucleus}$	Corrections (a) Time of flight	(b) Thick target	(c) Nuclear interaction	$\left(\frac{d^2\sigma^-}{dTd\Omega}\right)_{a,b} \times 10^{31}$ $\frac{cm^2}{Mev\text{-}Ster\text{-}Nucleus}$	$\left(\frac{d^2\sigma^-}{dTd\Omega}\right)_{a,b,c} \times 10^{31}$ $\frac{cm^2}{Mev\text{-}Ster\text{-}Nucleus}$
11.5	50	2.66 ± 0.25	1.17	1.12	1.01	3.47 ± 0.33	3.51 ± 0.34
28	112	3.79 ± 0.24	1.09	1.10	1.04	4.53 ± 0.29	4.73 ± 0.30
38	115	4.72 ± 0.47	1.08	1.06	1.08	5.40 ± 0.34	5.83 ± 0.37
56	109	5.92 ± 0.38	1.06	1.03	1.16	6.48 ± 0.42	7.50 ± 0.48
72	96	6.67 ± 0.46	1.08	1.02	1.23	7.31 ± 0.50	9.02 ± 0.62
91	97	4.79 ± 0.33	1.08	1.02	1.35	5.26 ± 0.45	7.10 ± 0.61
113	25	2.18 ± 0.29	1.07	1.02	1.52	2.38 ± 0.32	3.60 ± 0.45
133	1	0.15 ± 0.10	1.07	1.01	1.70	0.17 ± 0.12	0.29 ± 0.20
163	0	0.00 + 0.01	1.07	1.01	2.06	0.00 + 0.01	0.00 + 0.03

Based on 605 Star-Forming Negative Pions

$$\left(\frac{d\sigma^-}{d\Omega}\right)_{a,b,c} = (7.14 \pm 0.22) \times 10^{-29} \frac{cm^2}{Ster\text{-}Nucleus}$$

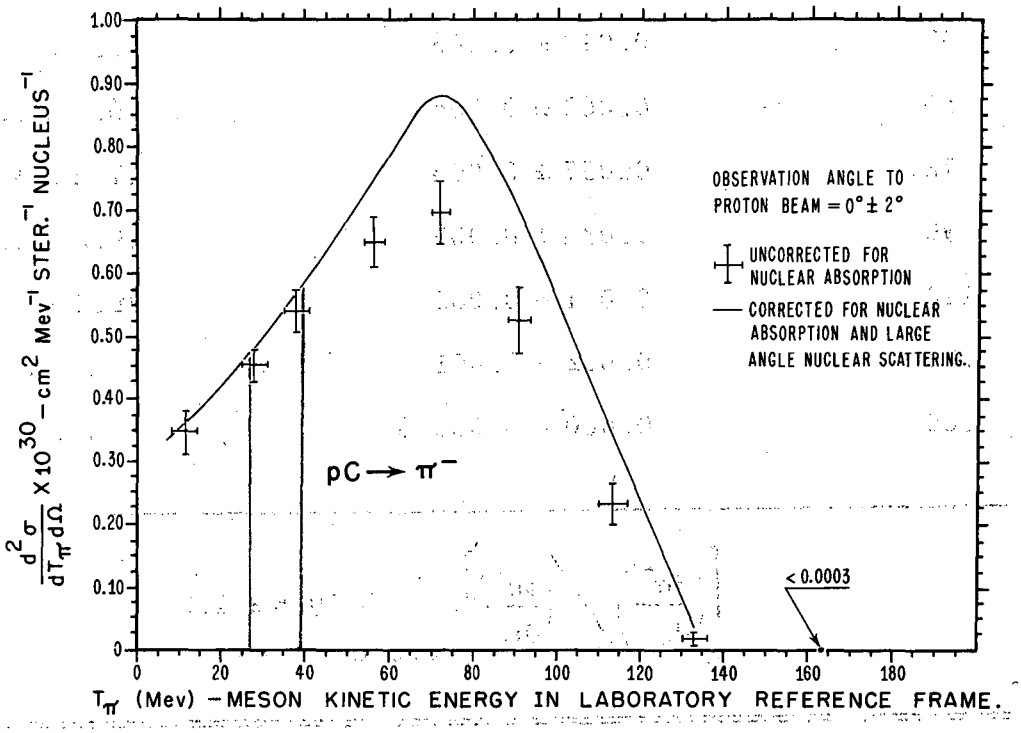

SPECTRUM OF PRODUCTION CROSS-SECTION FOR NEGATIVE π MESONS PRODUCED IN CARBON BY 340 Mev PROTONS.

MU-7629

Fig. 6.

Table V

Production Ratios for Positive and Negative Pions from Carbon at 0° to a 340-Mev Proton Beam

T_π (Mev)	$\left(\frac{d^2\sigma^-}{dTd\Omega}\right)\Big/\left(\frac{d^2\sigma^+}{dTd\Omega}\right)$	$\left(\frac{d^2\sigma^+}{dTd\Omega}\right)\Big/\left(\frac{d^2\sigma^-}{dTd\Omega}\right)$
15.5	0.086 ± 0.010	11.6 ± 1.4
37	0.077 ± 0.006	13.0 ± 1.1
56	0.062 ± 0.005	16.2 ± 1.3
72	0.057 ± 0.004	17.4 ± 1.4
90	0.034 ± 0.003	29.2 ± 2.4
112	0.021 ± 0.003	48.2 ± 6.9
132	0.002 ± 0.001	. . .
160	0.000 + 0.00006	. . .

$$\left[\left(\frac{d\sigma^+}{d\Omega}\right)\Big/\left(\frac{d\sigma^-}{d\Omega}\right)\right]_{a,b,c} = 29.5 \pm 1.2$$

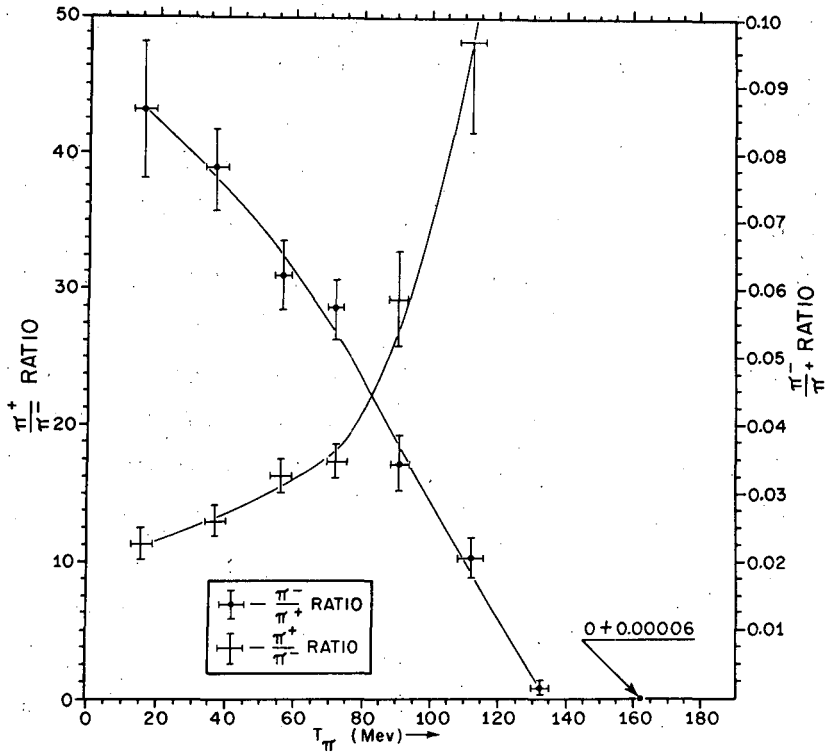

POSITIVE – NEGATIVE PION PRODUCTION RATIOS FROM CARBON AT 0° TO A 340 Mev PROTON BEAM.

MU-7021

Fig. 7.

C. Experimental Studies With A Spiral-Orbit Spectrometer

1. Some Facts Concerning the Spiral-Orbit Principle

The principle is based on the fact that a particular heterogeneous field can be created that is symmetric about the magnetic axis and gradually decreases as the distance from this axis is increased (references 7 through 13). If the axis of a cylindrical coordinate system (r, θ, z) is made to coincide with the axis of the magnetic field, then the equations for the components of this magnetic field can be represented as functions satisfying the following conditions:

$$H_r = H_r(r, z) = - H_r(r, z),$$

$$H_\theta = 0 \qquad H_z = H_z(r, z) = H_z(r, -z).$$

Furthermore, if a particular relation exists between the field strength and the momentum of a charged particle that is emitted radially in this field by a source that is centrally located in this symmetric magnetic field, the orbit of this particle converges to a definite circle. Therefore, this method of directional focusing permits high intensities to arise because of the large solid angle subtended by the detector, as all charged particles that are emitted in the (r, θ) plane and that satisfy the required momentum condition converge to the same circle. The circular orbit to which the particles converge is commonly referred to as the "stable orbit".

The conditions to be met by a particle that converges to the stable orbit can be derived in the following manner. Because of the axial symmetry of the magnetic field, the components of the field take on a simpler form when expressed in terms of the components of the vector potential. These are:

$$A_r = A_z = 0, \qquad A_\theta = A_\theta(r, z) = A.$$

It can be shown[33] that for the motion of a particle of charge -e in a static magnetic field, the appropriate Lagrangian is given by

$$\mathcal{L} = - m_o c^2 (1 - v^2/c^2)^{1/2} - \vec{ev} \cdot \vec{A}$$

where e is expressed in electromagnetic units. For our condition this expression takes the form,

$$\mathcal{L} = - m_o c^2 \left(1 - \frac{\dot{r}^2 + (r\dot{\theta})^2 + \dot{z}^2}{c^2} \right)^{1/2} - e r \dot{\theta} A \ .$$

Substituting this Lagrangian into the Langrange equations of motion, which are

$$\frac{d}{dt} \left(\frac{\partial \mathcal{L}}{\partial \dot{q}_i} \right) - \frac{\partial \mathcal{L}}{\partial q_i} = 0$$

where q_i represents any coordinate, one obtains the following three equations of motion:

$$m\ddot{z} = e r \dot{\theta} \frac{\partial A}{\partial z} \tag{8a}$$

$$m\ddot{r} = m r \dot{\theta}^2 - e \dot{\theta} A - e r \dot{\theta} \frac{\partial A}{\partial r} = m r \dot{\theta}^2 - e \dot{\theta} \frac{\partial}{\partial r} (rA) \tag{8b}$$

$$\frac{\partial \mathcal{L}}{\partial \dot{\theta}} = m r^2 \dot{\theta} - e r A = C_1 \tag{8c}$$

where C_1 is a constant of the motion, since $\frac{\partial \mathcal{L}}{\partial \theta} = 0$.

Equation (8c) can be modified to yield

$$U(r, z) = \frac{m r^2 \dot{\theta}^2}{2} = \frac{1}{2m} \left(\frac{C_1}{r} + eA \right)^2 = mQ,$$

where Q is an expression used in references 9 and 12, and U is now a scalar potential function in terms of which very simple relations can be obtained for the other two equations of motion. These are

$$m\ddot{r} = - \frac{\partial U}{\partial r} \quad \text{and} \quad m\ddot{z} = - \frac{\partial U}{\partial z} \ .$$

By multiplying these simple equations through by $\dot{r}$ and $\dot{z}$ respectively and adding, one obtains the relation

$$p_r^2 + p_z^2 + 2mU = p^2 \ . \tag{9}$$

As the momentum of the particle p is constant during the motion, then Eq. (9) is also a constant of the motion.

In particular, for the case of a particle that is emitted from the center of the coordinate system and moves in the plane (r, θ), it is easily verified that the following equations of motion,

$$(m\dot{r})^2 + 2mU = (mv)^2 \quad \text{or} \quad \dot{r}^2 = v^2 - \frac{e^2A^2}{m^2} \tag{10a}$$

and $$m r \dot{\theta} = eA, \tag{10b}$$

are satisfied as $z = 0$, $\dot{z} = 0$, and $C_1 = 0$. A particle that is governed by these equations of motion approaches a stable orbit at a radius $r = \rho$ if the following conditions are satisfied:

$$\text{(a) } \dot{r} = 0 \qquad \text{and} \qquad \text{(b) } \ddot{r} = 0 \; . \tag{11}$$

Condition (11a) combined with Eq. (10) yields

$$v = \frac{e}{m} A\,(r = \rho) \qquad \text{or} \qquad H(\rho) \cdot \rho = \frac{mv}{e} \; , \tag{12}$$

which defines the momentum of the particle that converges to the stable orbit. Condition (11b) requires that $\left(\frac{\partial A}{\partial r}\right)_{r = \rho} = 0$, i.e., that the value of A be a maximum at $r = \rho$. Hence from the relationship for the total flux $\phi = \int \vec{B} \cdot \vec{ds} = \oint \vec{A} \cdot d\vec{l}$ when evaluated at the stable orbit, we obtain

$$A\,(r = \rho) = \frac{1}{\rho} \int_0^\rho H(r)\, r\, dr$$

or

$$H\,(r = \rho) = \frac{1}{\rho^2} \int_0^\rho H(r)\, r\, dr \; . \tag{13}$$

As first pointed out by Iwata, Miyamoto, and Kotani,[9] Eq. (13) determines the radius ρ of the circle of convergence. Furthermore, Eq. (13) shows that the radius of convergence ρ depends on the shape of the magnetic field strength irrespective of the absolute value of the magnetic field. To summarize, a particle converges to the stable orbit at a radius $r = \rho$ if it satisfies the conditions stated in Eqs. (12) and (13).

The trajectory of the particle in the plane (r, θ) is determined by the relation $\theta = \int_0^r \frac{\dot{\theta}}{\dot{r}}\, dr$. This in turn can be expressed in terms of the parameters of the magnetic field as

$$\theta = \int_0^r \left[\left(\frac{mv}{eA} \right)^2 - 1 \right]^{-1/2} \frac{dr}{r} = \int_0^x \frac{a(x)}{\sqrt{1 - a^2(x)}} \frac{dx}{x}$$

$$= - \int_0^r \cot \lambda \frac{dr}{r} \qquad (14)$$

where $a(x) = \frac{A(r)}{A(\rho)}$, $x = \frac{r}{\rho}$ and $\cos \lambda = - \frac{A(r)}{A(\rho)}$. The angle λ is defined in Fig. 10.

2. Detailed Description of Experimental Method

a. Magnet and experimental procedure

The spectrometer that was employed in this experiment embodied in its design the knowledge gained in earlier studies with the spiral-orbit principle (references 7 through 13). It was constructed on a somewhat larger scale than any of its prototypes. A photograph illustrating its general over-all appearance is shown in Fig. 8.

The magnet for the 22-inch spiral-orbit spectrometer was designed so that the magnetic gap could be varied to a maximum of 14 inches. Furthermore, provisions were made to permit a wide choice of magnetic geometries. The particular geometry that was selected for this experiment is illustrated in Figs. 9, 11, and 13. For this geometry a continuous magnetic-field measurement was made, in the median plane across the entire pole face to a region 19 inches from the center of the magnet, by means of a bismuth probe method.[34] The magnetic field was then studied in the same manner at other angles to this direction. No appreciable eccentricity of the magnetic field distribution attributable to the return paths of the magnet was found. Each continuous field measurement was completely automatic with regard to distance and field-strength measurements. The accuracy of these relative field-strength measurements is better than 0.3%. The calibration for the bismuth probe was obtained by comparison with proton magnetic resonance in a uniform field at different field strengths. When the variation in field strength with radial distance was plotted, corresponding points along either of two opposite radii were found to coincide. The results obtained for the variation of the magnetic field strength with

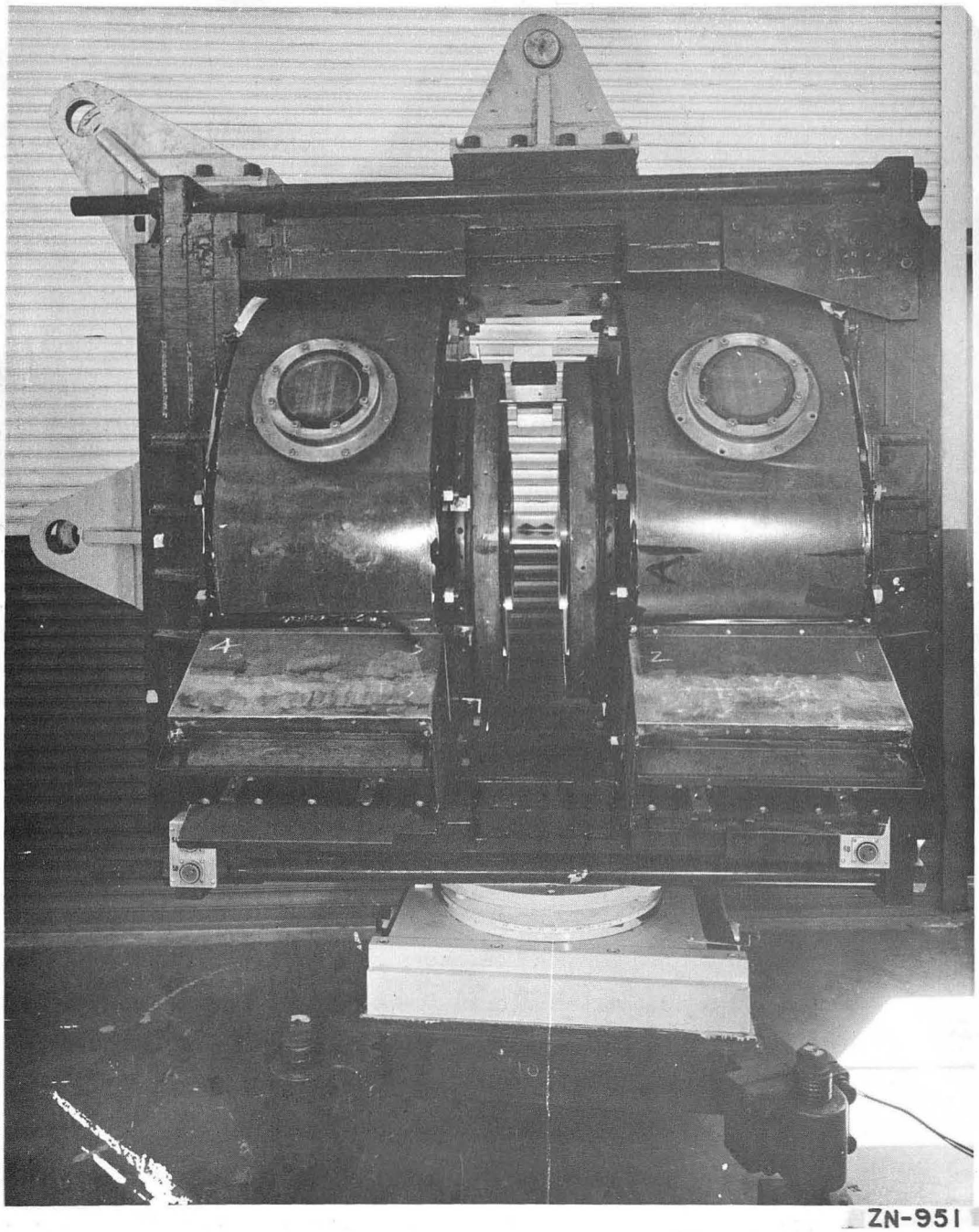

Fig. 8. Photograph of the spiral-orbit spectrometer. (22-inch)

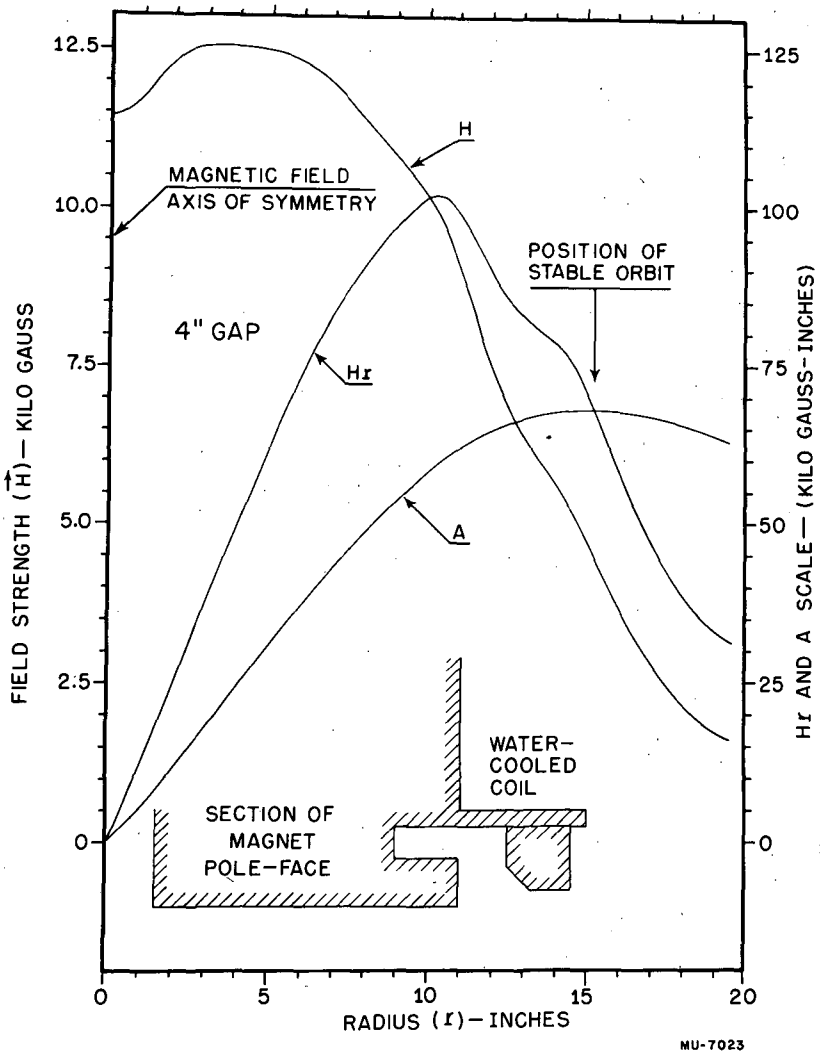

Fig. 9. Plots of magnetic field strength, vector potential, and Hr value against radius for a particular geometry of the spiral-orbit spectrometer.

radius are plotted in Fig. 9.

There are two methods for determining the position of the stable orbit for a charged particle whose motion is in the median plane of such a field: a graphic method and an analytic method.

(a) It is shown in Fig. 9 that the position of the stable orbit can be determined graphically from an intersection of a radial plot of two functions. The two functions are: (1) the product of the magnetic field strength H(r) at a point and the radius r at that point; (2) the vector potential A(r) of the magnetic field. As seen, it is a graphic way of establishing the conditions required by Eqs. (12) and (13). The position of the stable orbit determined by this method is $\rho = 15.20$ inches.

(b) The value of ρ can be obtained analytically, by first representing the magnetic field near the stable-orbit position by a polynomial in r. In this case a fourth-degree polynomial was chosen. For the interval ($13 \leq r \leq 17$) the magnetic field distribution can be represented by

$$H = a_o + a_1 r + a_2 r^2 + a_3 r^3 + a_4 r^4$$

where $a_o = 818,584$; $a_3 = -1077.94$;
$a_1 = -224,858$; $a_4 = 18.542$.
$a_2 = 23,370.4$;

The vector potential in this radial interval can now be expressed as

$$A(r) = \frac{1}{r} \int_0^{13} H \cdot r \, dr + \frac{1}{r} \int_{13}^{r} H \cdot r \, dr \quad .$$

Using Simpson's 1/3 rule to obtain the value of the first integral and substituting the expression for H into the second integral, one obtains

$$A(r) = \frac{b_{-1}}{r} + b_1 r + b_2 r^2 + b_3 r^3 + b_4 r^4 + b_5 r^5 \qquad (15)$$

where $b_{-1} = -5,375,987$; $b_3 = 5,842.595$;
$b_1 = 409,292$; $b_4 = -215.588$;
$b_2 = -74,952.7$; $b_5 = 3.090333$.

The value of $r = \rho$ that makes A(r) a maximum is obtained through established methods by first assuming a value of ρ and substituting this value into Eq. (15). This procedure is continued until the desired accuracy for ρ is established. Following such procedures a value of

ρ = 15.206 inches was obtained.

For this case the trajectories in the median plane of a particle emitted radially from the axis of magnetic symmetry were calculated by means of Eq. (14). These are illustrated for pions in Fig. 10. Such calculations are greatly simplified when the relation involving the angle λ is used.

b. Properties of a spiral-orbit spectrometer having a particular geometry: pion detection

Figure 10 partially illustrates the manner in which the spiral-orbit principle was applied for the measurement of the pion-production cross sections at 90° to the proton beam. The plotted pion trajectories demonstrate that a radial focusing exists for pions with a momentum specified by Eq. (12). Furthermore, because of the radial variation of the magnetic field, a vertical focusing is also introduced. These two focusing actions, as well as the rate of approach to the stable orbit by the trajectory of a pion emitted from a source at the center, are of prime importance in determining the pion intensity at the detector. One reason why the rate of approach is important can be seen in Fig. 10; this rate of approach greatly affects the solid angle subtended by the detector. In fact, a very slow rate of approach could cause the absorption of all pions having the required momentum by the shields protecting the detectors from direct background created at the target. Furthermore, because of the unstable nature of the pion, a slow rate of approach would decrease the pion intensity at the detector.

An insight into these three conditions is obtained from the work of Iwata, Miyamoto, and Kotani.[9] These authors have considered the problem of radial focusing based on the following boundary conditions:

(1) particles of velocity v that fulfill the conditions of convergence (Eqs. 12 and 13) are emitted uniformly in all directions in the plane z = 0 from the surface of a source of $r = r_o$,

(2) the center of the detector of width 2 d is set at a point on the stable orbit,

(3) the probability that a particle emitted at an angle α to the direction of r_o is collected in the detector is given by $I = \Theta/2\pi$, where Θ denotes the angle through which the particle stays in the annular

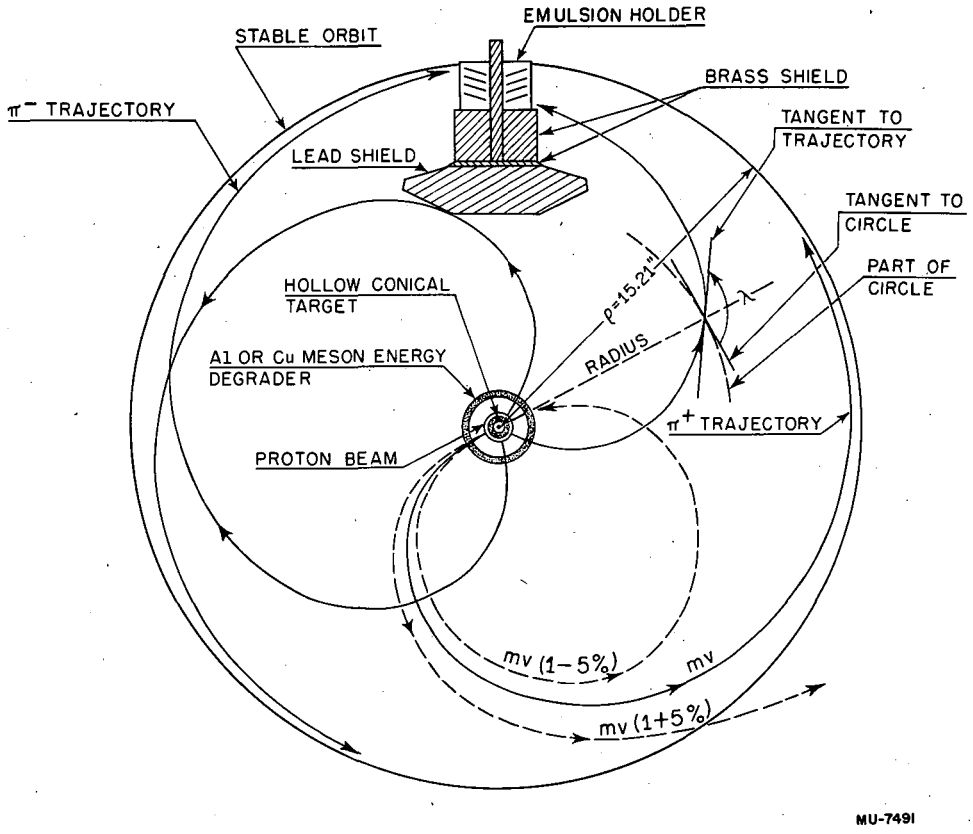

Fig. 10. Schematic illustrating application of the spiral-orbit principle to charged-pion detection. Pion trajectories are in the median plane of the magnetic field.

region defined by two concentric circles, of radius $(\rho - d)$ and $(\rho + d)$. For these conditions they report the following results:

(a) for $\frac{\Delta B}{B} + \frac{r_o}{\rho} \sin\alpha \geq 0$, i.e., for the case in which the particle never proceeds beyong the circle $r = \rho$,

$$I = \frac{K}{\pi\sqrt{2}} \cosh^{-1} \frac{d}{K\rho} \left(\frac{\Delta B}{B} + \frac{r_o}{\rho} \sin\alpha \right)^{-1/2} \qquad (16a)$$

(b) for $\frac{\Delta B}{B} + \frac{r_o}{\rho} \sin\alpha < 0$, i.e., for a particle that proceeds through the annular region,

$$I = \frac{K}{\pi\sqrt{2}} \sinh^{-1} \frac{d}{K\rho} \left(-\frac{\Delta B}{B} - \frac{r_o}{\rho} \sin\alpha \right)^{-1/2} . \qquad (16b)$$

In these equations B is the value of the vector potential $A(r = \rho)$ at the stable orbit while ΔB corresponds to the increment of variation of the vector potential from the value B in the neighborhood of the stable orbit. Furthermore, K is a constant, with a value near unity, that is defined only by the shape of the magnetic field distribution in the region of the stable orbit. It is introduced because the ratio $\frac{A(r)}{A(\rho)} = a(x)$, in the neighborhood of the stable orbit, can be expressed by the relation

$$a(x) = 1 - \frac{(1 - x)^2}{K^2} \quad ; \quad x = \frac{r}{\rho} \tilde{=} 1 \quad . \qquad (17)$$

As the rate of approach by the trajectory to the stable orbit depends on the field distribution in the region $r = \rho$, then this rate also depends on the value of K. It can be shown (using Eq. 14) that if $K > 1$ the trajectory gradually approaches the stable orbit, while if $K < 1$ the approach is much more rapid.

Iwata, Miyamoto, and Kotani[9] have also considered the two cases for a particle wherein: (a) the direction of emission has a small z component, and (b) the point of creation is not in the median plane. Their results illustrate that the z component of the trajectory oscillates about the median plane as the stable orbit is approached, according to the relation

$$z \sim \sin\left[a\left(\sqrt{1 + \frac{2}{K^2}}\right)\theta \right] .$$

From this expression it is evident that for $K \ll 1$ the period of this vertical oscillation is much shorter than the period of angular revolution, while for $K > 1$, this period may be comparable to or larger than the period of revolution. Therefore for $K > 1$, a particle distribution at the detector that is sharply peaked about the median plane is expected, while for $K < 1$ a nearly uniform distribution about the median plane should result. These conclusions have been verified experimentally.[25]

As the chosen method of detection for these experiments was a nuclear emulsion technique, the following properties of the spiral-orbit spectrometer were considered most desirable:

(a) a short pion-flight time, therefore a fast rate of approach by the trajectory to the circle of convergence ($K < 1$);

(b) a pion distribution at the detector that varies gradually with distance from the median plane ($K < 1$);

(c) a large pion-flux density ($K > 1$).

As the three conditions cannot be fulfilled simultaneously, the broad particle distribution at the detector was considered more desirable than the sharply peaked particle distribution. In this way if only a section of the emulsion was examined, a slight error in locating the same scanning region from emulsion to emulsion could be neglected, whereas for a sharply peaked distribution about the median plane it would be significant.

One can obtain the value of K for this experiment by expanding the vector potential in the neighborhood of the stable orbit in a Taylor series. This becomes

$$A(r) = A(\rho) - (\rho - r)\left(\frac{\partial A}{\partial r}\right)_\rho + \frac{(\rho - r)^2}{2}\left(\frac{\partial^2 A}{\partial r^2}\right)_\rho .$$

As previously stated, $\left(\frac{\partial A}{\partial r}\right)_\rho = 0$. Then comparing this expression with Eq. (17), one obtains

$$K^2 = -\frac{2A(\rho)}{\rho^2\left(\frac{\partial^2 A}{\partial r^2}\right)_\rho} = \frac{2RA(\rho)}{\rho^2} ,$$

where R is the radius of curvature of A(r) at the position of stable orbit. The value of R is readily obtained from Eq. (15). In this way it

was found that $K = 0.86$.

From the $H\rho$ value at $r = \rho$ one determines the energy of the monoenergetic pions that focus at the stable orbit. This pion energy is 9.2 Mev. As this is the practical upper limit of the magnetic field strength for the experimental geometry, one is forced to use hollow cylindrical energy degraders (Fig. 10) for the study of higher pion energies. For these higher pion energies the numerical values of the parameters that were considered by Iwata, Miyamoto, and Kotani[9] in their study of the behavior of the motion of a charged particle in a spiral-orbit spectrometer are no longer clearly defined. As an example, the value of r_o, which defines the surface from which the pion is emitted, becomes ambiguous. For 9.2-Mev pions a good approximation for r_o is a value of r obtained from an average taken over the thickness of the target. For the detection of pions of higher energies (for example, 40 Mev) r_o no longer has the numerical value that is used for the 9.2-Mev pion energy because the 40-Mev pions must first be degraded to 9.2 Mev before they can be focused at the stable orbit. Hence for these cases a truer value for r_o might be the radius of the surface of the cylindrical degrader (Fig. 10).

Because of these ambiguities a study was conducted on the radial and vertical focusing properties of the spiral-orbit spectrometer so that the results from these studies could be compared with the calculated predictions of Iwata, Miyamoto, and Kotani. Figure 11 illustrates schematically the experimental arrangement that was used for the detection of the pions during the radial focusing experiment; Fig. 13 illustrates the experimental arrangement employed during the vertical focusing experiment.

For the study of radial focusing (Fig. 11) a solid cylindrical carbon target (1 inch in outside diameter and 4 inches long) was mounted between the pole faces of the magnet with its axis coinciding with the axis of the magnetic field. The magnetic field strength was so set that pions having an energy of 8 Mev would be focused at the stable orbit. A collimated 340-Mev proton beam, circular in cross section and 1.3 inches in diameter at the target, was incident on the target along the magnetic axis of symmetry (Fig. 13). Pions that were created at 90° to this proton beam by proton-nucleus collisions and that were emitted

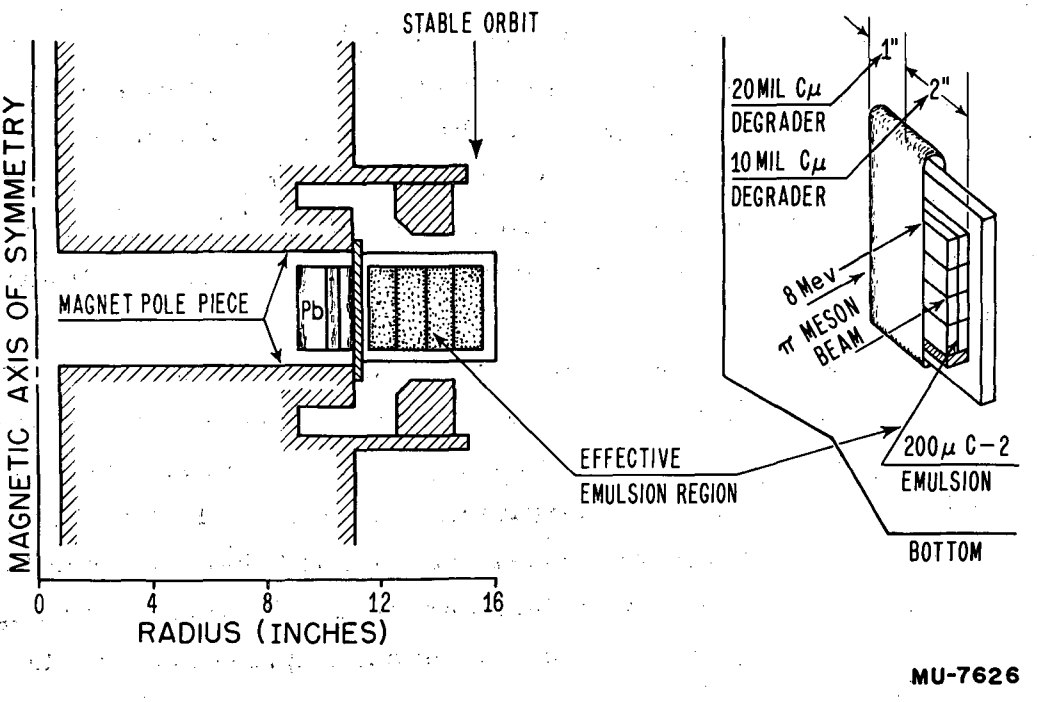

Fig. 11. Schematic of experimental arrangement for studying radial focusing in a spiral-orbit spectrometer.

from the surface of the target with an energy of 35 Mev were degraded in energy by a copper attenuator to 8 Mev (Figs. 10 and 13). These pions were then detected by nuclear emulsions arranged as illustrated in Fig. 11. The monoenergetic pions entered the detector perpendicularly. Copper was used to attenuate the 8-Mev energy of the pions just prior to detection. Because their projected range in copper (for which no integral range curves for 8-Mev pions exists) was not known, two different thicknesses of Cu were used, side by side. In every case eight 1 x 3-inch emulsions were exposed simultaneously. As shown in Fig. 11, the emulsion was always sandwiched between two glass surfaces.

It was pointed out in the calculations of Iwata, Miyamoto, and Kotani[9] that if all spiral-orbit parameters were fixed and the value r_o varied, the peak intensity at the detector would decrease as r_o increased. Therefore four radial-focusing experiments were made. During these experiments all the spiral-orbit conditions were fixed while the outer diameter of the cylindrical copper degrader was varied. The four experimental values of the outer diameter were 2.5 inches, 4.0 inches, 6.0 inches, and 8.0 inches. The effect on radial focusing of these first three degraders is shown in Fig. 12 a. The radial focusing for the 2.5-inch-diameter degrader was analyzed in more detail. These detailed results and their standard deviation are summarized in Fig. 12 c. From these studies on radial focusing one can conclude that:

(a) a similar shape is obtained for the intensity distribution near the stable orbit, as is predicted by Eq. (16),

(b) the peak intensity undergoes a small shift in position as the diameter of the degrader is increased,

(c) a large increase in the diameter of the degrader markedly affects the value of the peak intensity,

(d) the peak intensity occurs at a value of r that is smaller than the calculated value of the stable orbit.

For the study of vertical focusing the same target and method of pion production were used. In this particular case the magnetic field strength was increased so that pions having an energy of 9.2 Mev were

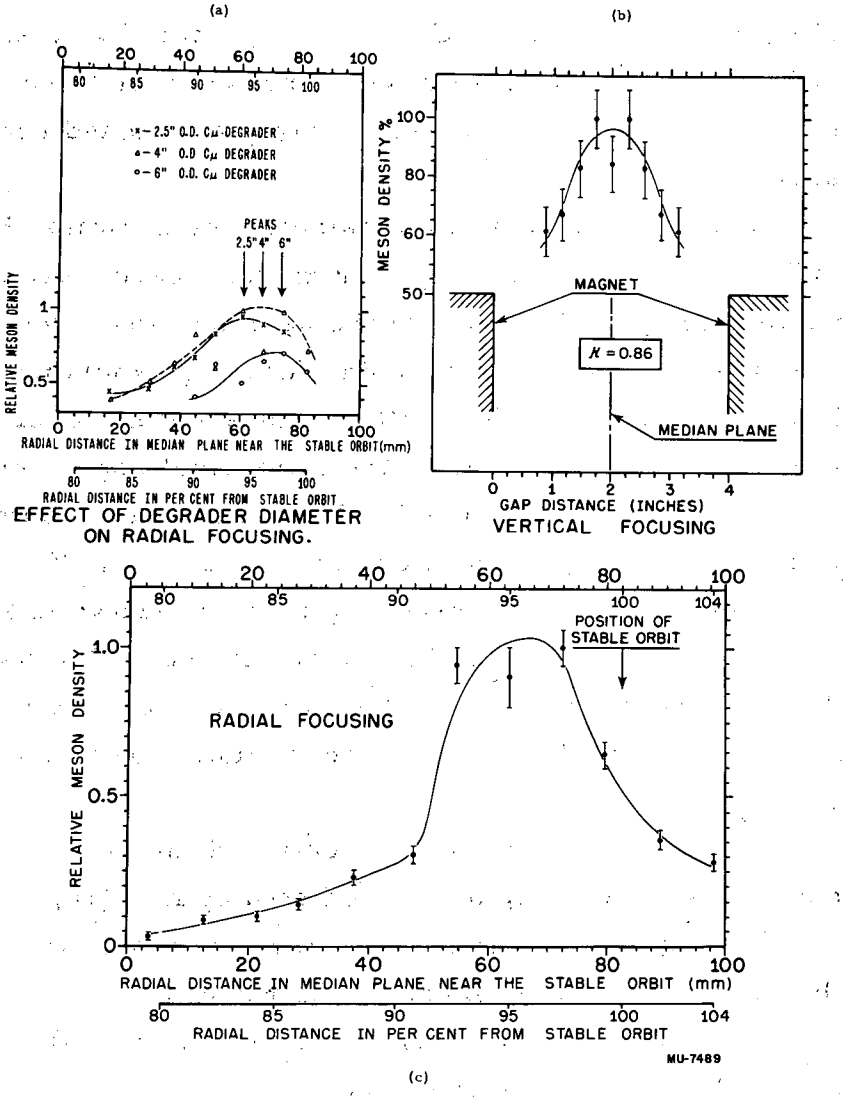
(a)
(b)
x – 2.5" O.D. Cμ DEGRADER
Δ – 4" O.D Cμ DEGRADER
o – 6" O.D. Cμ DEGRADER
PEAKS
2.5" 4" 6"
RELATIVE MESON DENSITY
RADIAL DISTANCE IN MEDIAN PLANE NEAR THE STABLE ORBIT(mm)
RADIAL DISTANCE IN PER CENT FROM STABLE ORBIT
MESON DENSITY %
MAGNET
K = 0.86
MEDIAN PLANE
GAP DISTANCE (INCHES)
VERTICAL FOCUSING
EFFECT OF DEGRADER DIAMETER ON RADIAL FOCUSING.
POSITION OF STABLE ORBIT
RADIAL FOCUSING
RELATIVE MESON DENSITY
RADIAL DISTANCE IN MEDIAN PLANE NEAR THE STABLE ORBIT (mm)
RADIAL DISTANCE IN PER CENT FROM STABLE ORBIT
MU-7489
(c)

Fig. 12.

focused at the detector. The method of detection is illustrated in Fig. 13. For this study the 9.2-Mev pions were incident on an emulsion holder containing four nuclear emulsions that were inclined at 15° to the direction of the pion beam (Fig. 14a). (The reasons for this angular inclination have been considered above in the discussion of the poor-geometry experiment.) This method of pion detection was chosen for the study of vertical focusing because it was the one adopted for the measurement of the pion-production cross sections at 90° to the proton beam. The emulsions were exposed in the region of peak intensity as found from the study of radial focusing. The results on vertical focusing are plotted, with their standard deviations, in Fig. 12b. From these results one concludes that the desired broad spread of pion distribution about the median plane, predicted by the theory for $K < 1$, was obtained.

The method of detecting the almost monoenergetic and nearly parallel beam of pions was quite different from that previously described in the poor-geometry experiment. As was pointed out, there are many factors known to affect the range of a monoenergetic pion beam. To insure that the pion density in emulsion was not reduced appreciably by the wrong choice of thickness of the final degrader (Fig. 14a), a portion of the projected range-straggling curve in aluminum near the value of the calculated mean range was obtained for 9.2-Mev pions. The results of these measurements are plotted in Fig. 14b. Also shown in Fig. 14b are the calculated mean range of 9.2-Mev pions and the actual experimental thickness that was used with the emulsion holder (Fig. 14a) for pion detection during the experiment. This method of detection also gives rise to a distribution of pion densities in the emulsion, as each increment of emulsion volume subtends a different solid angle at each point of the final degrader. The behavior of this density distribution, obtained from approximately 10,000 pions, is shown in Fig. 14c. This pion-density distribution in emulsion aided greatly in the study of large π^+/π^- ratios, as a positive-pion region could always be found in which the pion density was not so great as to make accurate scanning difficult.

All these factors affecting the pion intensity at the detectors were taken into account in determining the final position of the pion detector

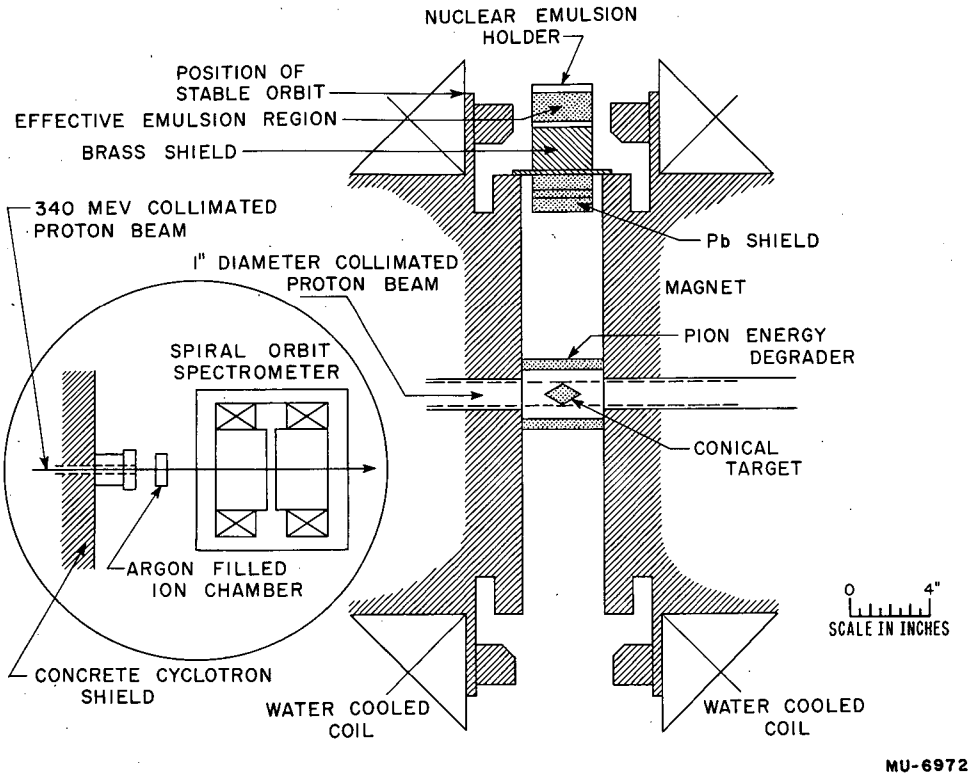

Fig. 13. Schematic of experimental arrangement in spiral-orbit spectrometer for studying vertical focusing and pion production.

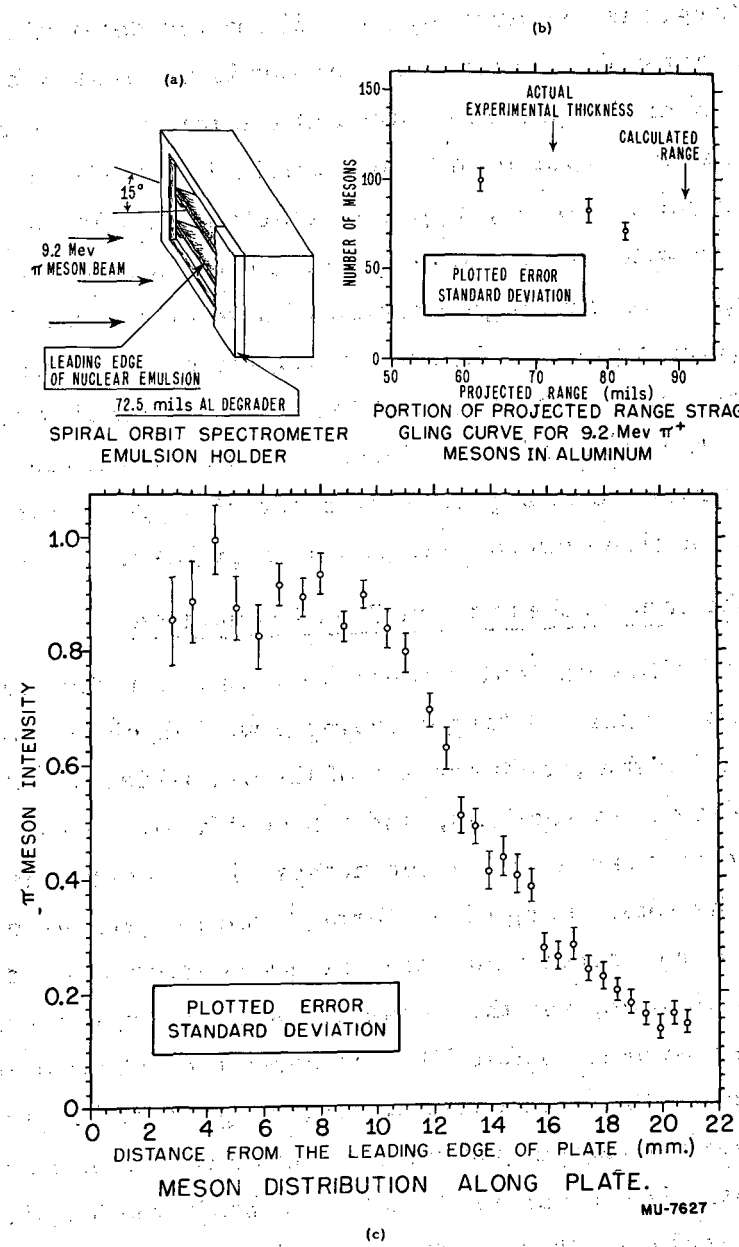
(a)
15°
9.2 Mev
π MESON BEAM
LEADING EDGE
OF NUCLEAR EMULSION
72.5 mils AL DEGRADER
SPIRAL ORBIT SPECTROMETER
EMULSION HOLDER
(b)
ACTUAL
EXPERIMENTAL THICKNESS
CALCULATED
RANGE
NUMBER OF MESONS
PLOTTED ERROR
STANDARD DEVIATION
PROJECTED RANGE (mils)
PORTION OF PROJECTED RANGE STRAGGLING CURVE FOR 9.2 Mev π+
MESONS IN ALUMINUM
π MESON INTENSITY
PLOTTED ERROR
STANDARD DEVIATION
DISTANCE FROM THE LEADING EDGE OF PLATE (mm.)
MESON DISTRIBUTION ALONG PLATE.
MU-7627
(c)

Fig. 14.

for the pion-production studies. As is illustrated in Figs. 10 and 13, this position is considerably below the calculated value for the stable orbit.

It was pointed out by Miyamoto[8] that the alignment of the source with the axis of the magnetic field was essential for the success of this type of spectrometer. Furthermore, very accurate alignment of the target is required by Eq. (2) for the determination of the geometric factor C_2. This requirement is necessary because the proton flux over the projected area of the target is not uniform. Even though in this experiment some ambiguity exists as to what constitutes the source (i.e., r_o), nevertheless, a special target holder was made with which the target could be mounted very accurately with regard to the magnetic axis of symmetry and also with regard to the median plane. Figure 15 illustrates the main features of the target holder and the shape of the hollow conical targets that were used for the production studies. The hollow conical targets permitted the exposure of a greater number of target nuclei to the proton beam for a given proton and pion energy loss.

3. Experimental Results on Pion Production

Two hollow conical targets were used for the study of the entire energy spectrum. A target having a wall thickness of 0.360 g/cm^2 was used for the measurement of the 12.5-Mev and 27-Mev pion-production cross sections, and a target having a wall thickness of 0.720 g/cm^2 was used for the higher pion-energy measurements.

As the total energy loss through the target was more significant for the energy spread than the energy resolution of the spectrometer, this was adopted, for the present, as the energy resolution of the measured values. Table VI illustrates the behavior of the energy resolution of the spectrometer for this geometry. These estimated values were obtained graphically from Fig. 10 merely to illustrate this point. These values do not take into consideration the effect on energy resolution that is introduced by the energy degrader. This effect is still to be considered and is not covered in this report.

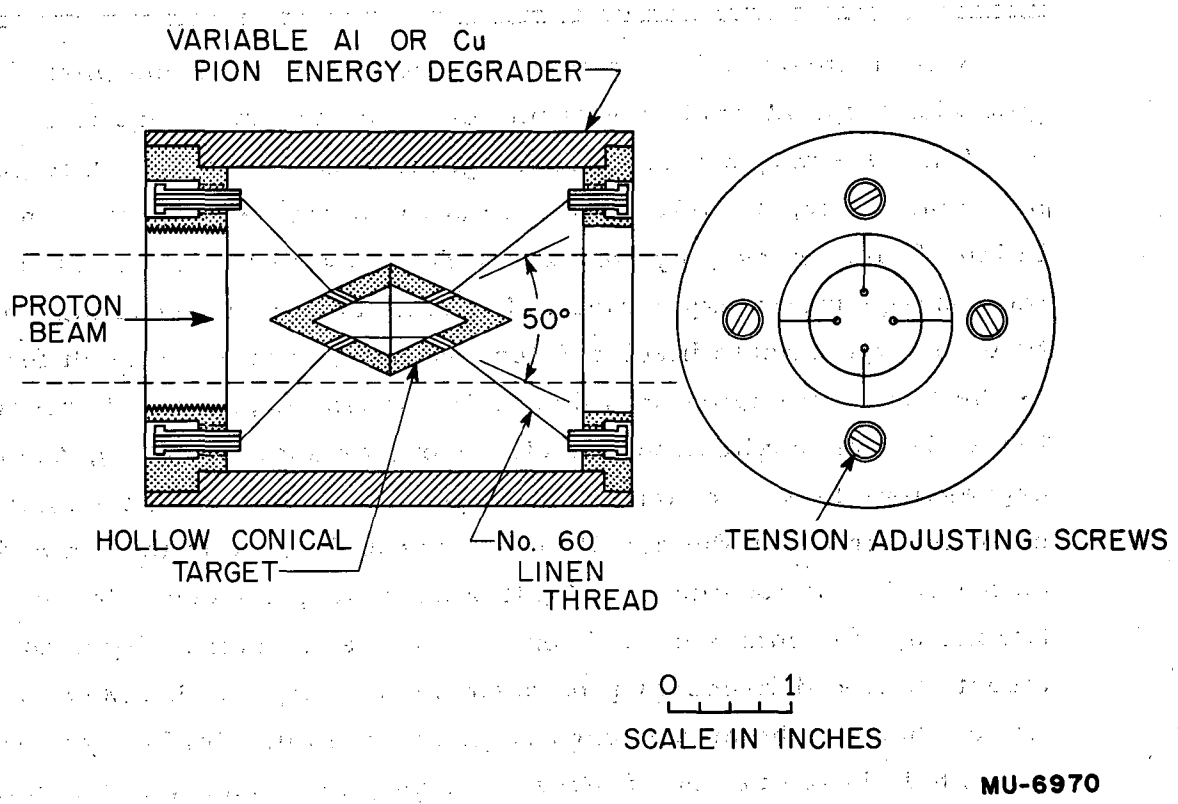

Fig. 15- Illustration of target holder and hollow conical pion-production target.

Table VI

Illustration of Spiral-Orbit Spectrometer Energy Resolution

Momentum of the pion in terms of $H\rho$ value	T_π (Mev)	Relative collection intensity (%)
$H\rho + 10\% H\rho$	11.1	3.7
$H\rho + 5\% H\rho$	10.1	5.7
$H\rho + 2\% H\rho$	9.5	8.4
$H\rho + 1\% H\rho$	9.35	12
$H\rho$	9.2	100
$H\rho - 1\% H\rho$	9.0	4.6
$H\rho - 2\% H\rho$	8.85	0

Measurements of relative cross sections at different pion energies with a spiral-orbit spectrometer require a knowledge of C_2 in Eq. (2). One may obtain some insight into the meaning of this geometrical factor, as well as an estimation of its behavior with the variation of pion energy, by comparing Eq. (2) with Eq. (7) obtained from the poor-geometry experiment. It should be remembered that the two types of experiments involve detection methods that are as different as the basic principles on which their success depends. However, for a first approximation (for pion energies above 25 Mev), the two expressions may be equated for the purpose of obtaining a numerical value for C_2 on the condition that the difference in the method of detection is not considered. On this condition, the equivalence of the two methods becomes clear if one considers the similarity in the attenuation of a high-energy pion beam to an energy of 9.2 Mev by the two methods. The pion-energy region where this similarity is expected to hold is the region of large f values (i.e., nearly equal to unity), where $f = x/R$, R being the mean range of the pion in the absorber, and x the thickness of absorber that is necessary to attenuate the original pion energy T_i to 9.2 Mev. Under these conditons one obtains the expression

$$C_2 = \frac{C_3}{\left(-\frac{dT}{dR}\right)_{T_i} \frac{R_{ab}}{R_{em}}\Big|_{9.2} \frac{d\Omega}{dA}} , \qquad (18)$$

where C_3 is a constant that depends on the uniformity of the proton beam at the target. For targets that can be accurately mounted and that have the same projected area to the direction of the proton beam, the constant C_3 will be the same for all targets and pion energies. Now, $(R_{abs}/R_{em})_{9.2}$ is a constant; and if: (a) the scanning area remains the same and (b) the solid angle of the spectrometer remains constant as the pion energy is varied, then C_2 depends only on the rate of energy loss in the main energy degrader by a pion having an initial energy T_i. That is,

$$C_2 = \frac{K}{\left(\frac{dT}{dR}\right)_{T_i}} \quad . \tag{19}$$

Here K is a constant whose value depends on the solid angle. This value changes in a nonuniform proton beam if the proton beam position is varied with respect to the target. Therefore, in order to measure relative production cross sections with a spiral-orbit spectrometer, it is essential to establish the behavior of K as the thickness of the main energy degrader is varied.

At first, only one method was available for making these measurements. (Another is now being used.) This original method consisted of studying the spectrum of positive-pion production from carbon with the spiral-orbit spectrometer, and comparing these results with the results presented in Table II. This study of the constancy of K is permissible if the target, the proton beam, and the position of the detector, are fixed for all pion energies. The results of this study are presented in Table VII. The tabulated error is the accumulated standard deviation.

These results illustrate that the solid angle of the spiral-orbit spectrometer remains constant for pion energies above 25 Mev even though an energy degrader is introduced. From a consideration of these results and also the theoretical calculations on the resolution of the spiral-orbit spectrometer[9], a conclusion was reached by Dr. R. Sagane and the writer that the solid angle may remain constant for pions of energies smaller than 25 Mev. This conclusion, that the solid angle is constant throughout, demands an explanation for the observed deviation from a constant solid angle at a 12.5-Mev pion

energy. It is our present belief that Eq. (7) derived for the poor-geometry experiment is not applicable to such regions of low pion energy. To test these conclusions a more refined method, involving a 40-inch spiral-orbit spectrometer, is being used. (This method, however, is not discussed in this report.)

Table VII

Effect of an Energy Degrader on the Solid Angle of a Spiral-Orbit Spectrometer

T_π (Mev)	No. of observed pions	Relative value of C_2	Relative value of K
12.5	497	1.00 ± 0.15	0.73 ± 0.11
25	494	2.20 ± 0.26	0.97 ± 0.12
37	429	3.21 ± 0.32	1.14 ± 0.12
57	483	3.58 ± 0.26	1.00 ± 0.07
72	204	4.00 ± 0.53	1.00 ± 0.13

Because of the ambiguity concerning the solid angle in the regions of low pion energy, the π^--production cross sections from carbon at 90° to the proton beam are obtained by direct multiplication of the measured π^-/π^+ values and the observed π^+-production cross sections (Table II). Table VIII summarizes the results that were obtained on pion production from carbon. The number of observed positive pions and the number of observed star-forming negative pions are tabulated at each point. In some cases the reported π^+/π^- or π^-/π^+ results are not obtained directly from the number of observed pions and the application of the zero-prong correction factor of 1.35 for the starless negative pions. An additional normalization factor for positive pions must be used to take account of the variation of pion density in the emulsion. This factor was previously mentioned in connection with Fig. 14C. The same notation is used as in Table I. The reported error is the statistical probable error.

These data are also presented in graphical form. Figure 16 represents a plot of the π^--production cross sections, and a plot of the

Table VIII

Charged-Pion Production Data from Carbon at 90° to a 340-Mev Proton Beam

T_π (Mev)	Observed no. of π^+ mesons	π^+ normalization factor	Observed no. of star π^- mesons	π^+/π^- Ratio	π^-/π^+ Ratio	$\left(\frac{d^2\sigma^-}{dT_\pi d\Omega}\right)_{a,b} \times 10^{31}$ ($cm^2 Mev^{-1} Ster^{-1} Nucleus^{-1}$)	$\left(\frac{d^2\sigma^-}{dT_\pi d\Omega}\right)_{a,b,c} \times 10^{31}$ ($cm^2 Mev^{-1} Ster^{-1} Nucleus^{-1}$)
12.5 ± 2	872	1.000	145	4.46 ± 0.23	0.224 ± 0.012		
16.5 ± 2					0.202 ± 0.013	8.71 ± 0.68	8.85 ± 0.69
25 ± 1.5	1602	1.678	296	6.70 ± 0.25	0.149 ± 0.006	7.50 ± 0.68	7.80 ± 0.69
37.5 ± 2	1455	1.415	161	9.44 ± 0.46	0.106 ± 0.005	5.10 ± 0.30	5.50 ± 0.33
57 ± 2	895	1.090	59	12.20 ± 0.96	0.082 ± 0.006	2.61 ± 0.23	3.07 ± 0.27
72 ± 2	675	1.000	32	15.9 ± 1.7	0.063 ± 0.007	1.30 ± 0.16	1.61 ± 0.20

$$\left(\frac{d\sigma^-}{d\Omega}\right)_{a,b,c} = (4.27 \pm 0.20) \times 10^{-29} \ cm^2 Ster^{-1} Nucleus^{-1}$$

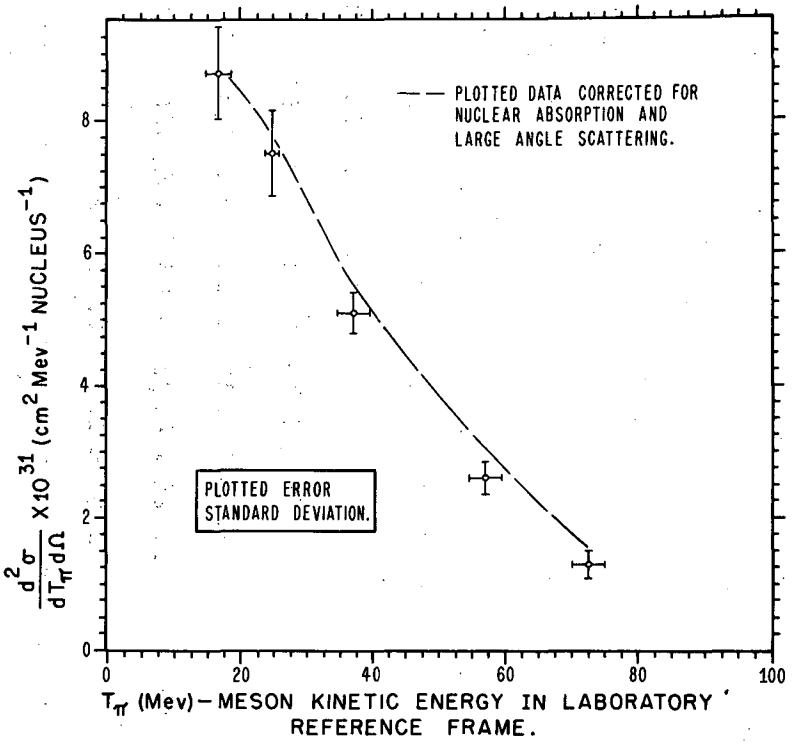

SPECTRUM OF PRODUCTION CROSS-SECTIONS FOR NEGATIVE PIONS FROM CARBON AT 90° TO A 340 Mev PROTON BEAM.

MU-7628

Fig. 16.

ratios is presented in Fig. 17. The plotted ratios show good agreement with previously reported measurements[13]. The area $\left(\frac{d\sigma^-}{d\Omega}\right)_{a,b,c}$ under the curve for $\left(\frac{d^2\sigma^-}{dTd\Omega}\right)_{a,b,c}$ was obtained by means of a histogram and is presented in Table VIII. It should be noted that because of the steep rise in the π^- cross section as the pion energy is lowered, an error can easily be introduced into the reported value for $\left(\frac{d\sigma^-}{d\Omega}\right)_{a,b,c}$ by an erroneous assumption concerning the behavior of the cross section at low pion energies. To determine this value it was assumed that the π^--production cross section does decrease at some lower pion energy. A discussion of this follows.

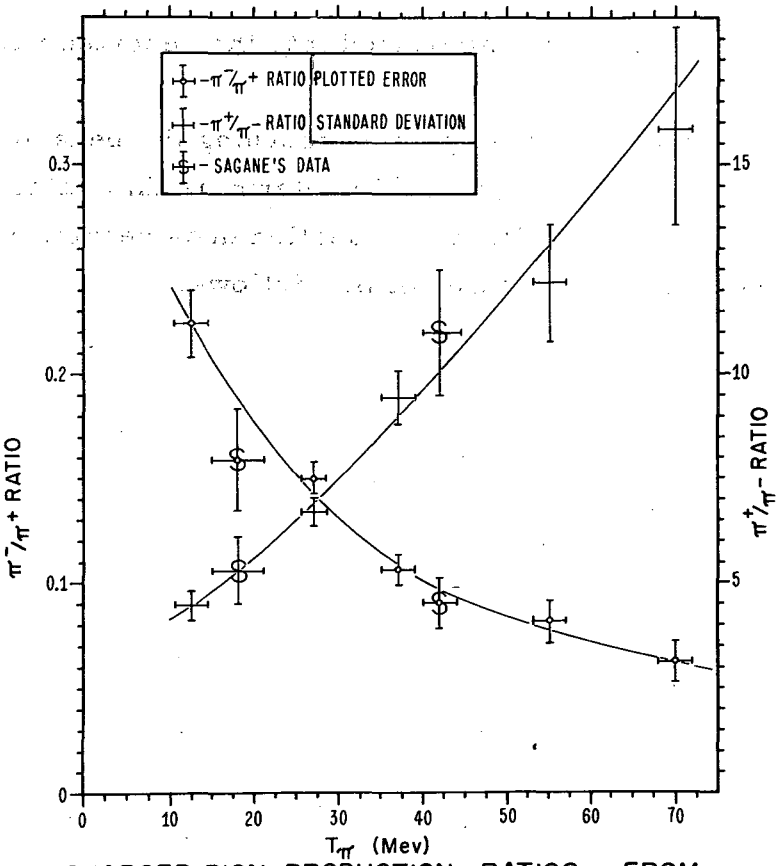

CHARGED PION PRODUCTION RATIOS FROM CARBON AT 90°TOA340 Mev PROTON BEAM

MU-7625

Fig. 17.

IV. DISCUSSION

A. Production of Positive Pions from Carbon at 90° to the Proton Beam

Since the appearance of a second experiment on π^+ production from carbon at 90° to the proton beam[2], a great deal of discussion has taken place on the possible reasons for the disagreement between these results and the results of an earlier experiment[19, 5] on the same element. As this same experiment is presented in this report, it is only proper to compare the results of the three experiments and to consider the possible reason for the disagreement between the data from Passman, et al.[2], and the data reported by Richman and Wilcox.[19] For some time it has been the general belief that the two equations (as reported in (a) of reference 2 and (b) of reference 1, or in Eq. (7) in this report) by which the cross section was calculated in the two experiments were truly different. That different values would be obtained from the two equations by treating the same data was also illustrated.[14] Therefore, it is important to consider the two equations in detail and to investigate the region of their application, especially since evidence from the experiment on the solid angle of the spiral-orbit spectrometer has cast some doubt on the validity of Eq. (7) in the region of low pion energy. It should be pointed out that in the experiment on the solid angle of the spiral-orbit spectrometer the assumption was made that Eq. (7) is true for all pion energies. One may now reverse the assumption (as there are good reasons for its validity), i.e., assume that the solid angle of the spiral-orbit spectrometer is constant. In this case the constancy of the value K in Table VII is a check on the validity of Eq. (7).

A comparison of the two equations in questions reveals that they are identical except for one parameter. The equation as it was used by Passman, et al., involved the stopping power of emulsion. This will be referred to as $\left[\left(\frac{dT}{dR}\right)_{em}\Big|_{T_i}\right]_{col}$. In the work by Richman and Wilcox (i.e., Eq. (7) in this report), this stopping power of the emulsion was replaced by the product of a constant that depends on the absorber (Fig. 18b), and the stopping power of the absorber, i.e.,

by $\left[\left(\frac{dT}{dR}\right)_{abs}\Big|_{T_i}\frac{R_{abs}}{R_{em}}\Big|_{T_m}\right]$. Use was made of this second expression because at the time no information was available from which to obtain accurate values of the stopping power for emulsion in the desired pion-energy region. One arrives at both of these factors in a similar way, i.e., they arise from the derivation of a relation between (a) the total number of pions of energy T_i per cm^2 per Mev that are incident on the face of the absorber that contains the nuclear emulsion, and (b) the density of these pions at this energy in the emulsion (see Eq. (6)). Let us re-explore the assumptions on which they depend. Since the assumptions are the same in the two cases, a discussion of only one of them is necessary.

One can see that Eq. (6) follows because of a relation that was obtained after Eq. (5) was averaged over all possible values of T'. In this averaging process the assumption was made that T_i was much larger than T_m and that the expression $\left[\left(\frac{dT}{dR}\right)_{T_i}\Big|_{abs}\right]$ was therefore essentially constant during the averaging process. As a result, Eq. (6) is true only under this condition. This same condition applies to $\left[\left(\frac{dT}{dR}\right)_{em}\Big|_{T_i}\right]_{col}$, as this relation is obtainable by similar arguments. One arrives at this last expression by replacing the absorber that contains the emulsion with a volume of emulsion having the same effect on energy attenuation. That this is permissible follows from the very definition of the Bethe stopping-power formula,[41] as the stopping power is dependent on the total number of electrons per cubic centimeter and the average excitation potential of the atom. As the emulsion is a composite structure, the stopping power of emulsion is a summation of the individual stopping powers of each of its elements. For high energies a small error is introduced into these calculations because of the density effect[37] on the stopping power of different materials. The density effect is larger for materials having the smaller atomic numbers. This effect, which is the reduction in the ionization loss of a charged particle because of the polarization

of the medium, it too small,[37] however, to be considered for the pion-energy region under discussion (i.e., for $T_i \leq 100$ Mev).

To summarize: the two equations for calculation of the cross sections in the two experiments in question are equivalent, and therefore the ratio $\left[\left(\frac{dT}{dR}\right)_{abs} \frac{R_{abs}}{R_{em}}\right] \Big/ \left[\left(\frac{dT}{dR}\right)_{em}\right]_{col}$ should equal unity for at least those pion energies that satisfy the condition under which Eq. (6) is valid.

The desired stopping-power values were calculated in the manner stated by the authors of the two experiments. From these determined values this ratio was obtained; it is plotted for different pion energies in Fig. 18a. As shown, this calculated ratio is not the constant one, but a function of pion energy. Because of this dilemma the method used by the authors for evaluating the stopping power of emulsion was questioned. This stopping power was calculated by modifying in the conventional manner the experimental range-energy curve[42] for protons in Ilford C-2 emulsions; i.e., from R(in microns) = 41.8 $T^{1.722}$(in Mev). As the original experimental range-energy curve was established for protons up to an energy of 40 Mev, there was reason to doubt the validity of the applied extrapolation of this relation (up to a 775-Mev proton energy) from which the stopping power was determined. Furthermore, because a differentiation of this range-energy expression is necessary to determine the stopping power, the error in the calculated stopping power is much greater than the corresponding error in range. For these reasons, the calculations of the stopping power of C-2 emulsions as presented by Vigneron[36] were extended into the desired energy region in the conventional manner. These extended calculations also included the density effect correction.[37] The ratios involving the expression $\left[\left(\frac{dT}{dR}\right)_{em}\Big|_{Vigneron}\right]$ for the stopping power of emulsion were recalculated and are plotted in Fig. 18a. As seen, this ratio remains unity for the desired pion-energy region. It might be pointed out that the calculated values of the ranges for protons in C-2 emulsions as reported by Vigneron are in excellent aggreement with new experimental results, i.e., for 33-Mev protons[43] and for 340-Mev protons.[44]

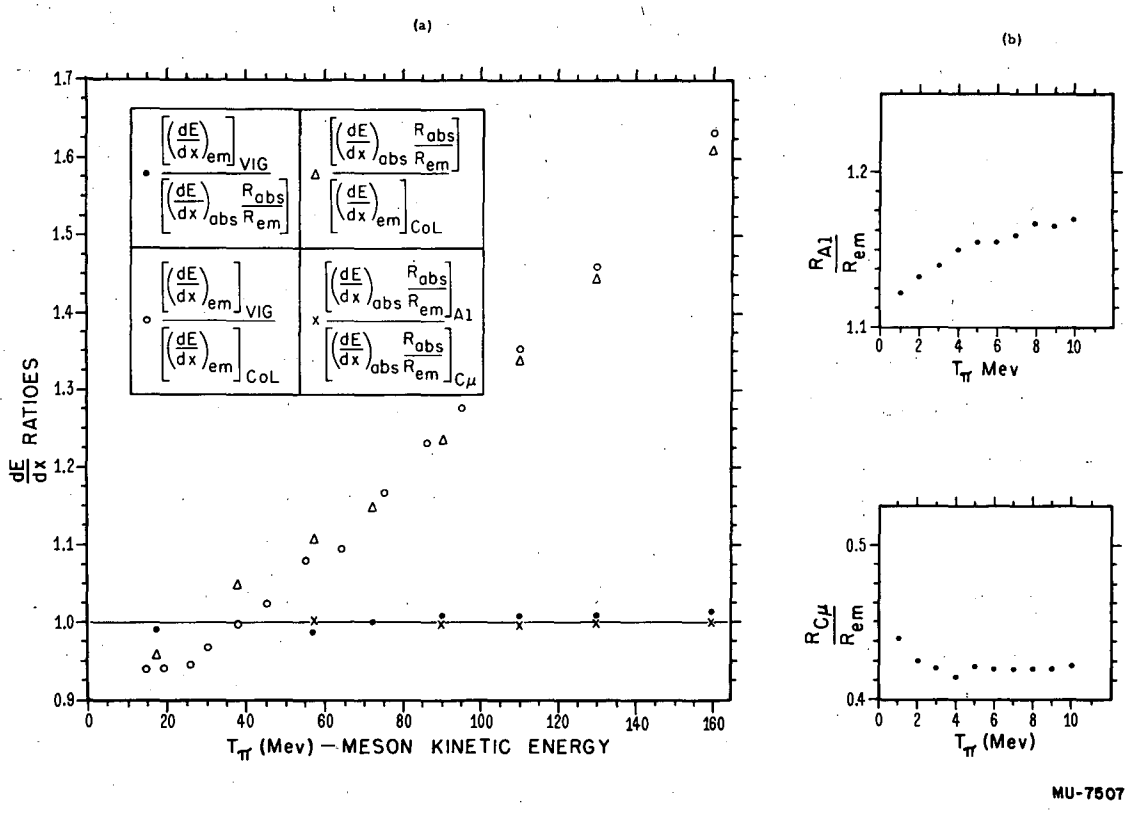
(a)
(b)
dE/dx RATIOES
T_π (Mev) — MESON KINETIC ENERGY
R_A1/R_em
T_π Mev
R_Cμ/R_em
T_π (Mev)
MU-7507

Fig. 18.

On the basis of these considerations the original data of Passman, et al.,[2] were corrected to $\left[\left(\frac{dT}{dR}\right)_{em}\Big|_{Vigneron}\right]$ by a factor that is plotted in Fig. 18a. The effect of this correction on the data of Passman, et al., is shown in Fig. 19, where their original data are reproduced. Figure 18a also illustrates that no error is introduced into the results presented in this report by changing from aluminum emulsion holders to copper.

Appearing in Fig. 19 are the plots of all experimental data on π^+ production from carbon at 90° to a proton beam having an approximate proton energy of 340 Mev (data of Passman, et al., are reported at 345 Mev). It should be pointed out that Hamlin's counter data were reproduced as reported[35] except for the change in the scale of the ordinate. These counter data were fitted by Hamlin to the emulsion data presented in this report by using a normalization factor obtained from the areas under the two curves. Hamlin did not state the energy resolution in his report; however, it is larger than the energy spread at corresponding points as presented in this report. It might also be mentioned that a similar normalization of the counter data to the original results of the other experiments does not lead to the good agreement on the shape of the spectrum that is found between the Hamlin[45] and Dudziak results (Fig. 19). As seen in Fig. 19, if the proposed correction to the data of Passman, et al., is permitted, then all information on π^+ production from carbon at 90° to the proton beam is generally in good agreement in the region of high pion energies.

A large disagreement between the three experimental results still remains in the region of low pion energies, even though the above correction is permitted. To summarize, there are several factors that will affect the cross section at low energies. How each of these was accounted for by the different experimenters is difficult to judge, and it is even more difficult to attempt an estimate of the proper correction factor that might be applied to the different data. As was pointed out, the change in the value of K in Table VII in this energy region casts some doubt on the validity of Eq. (7) and its counterpart in the experiment of Passman, et al. That there is cause for

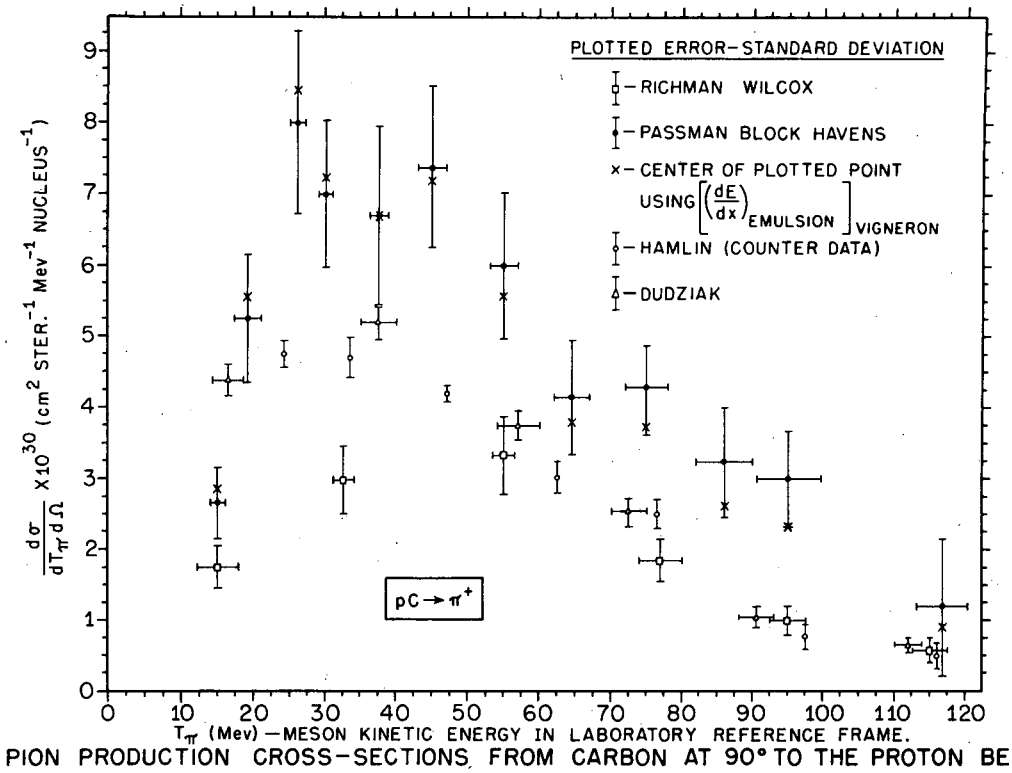

PION PRODUCTION CROSS-SECTIONS FROM CARBON AT 90° TO THE PROTON BEAM.

MU-7487

Fig. 19.

this doubt is clearly seen from the derivation of Eq. (6) and its counterpart in the Passman experiment. The necessary condition for Eq. (6) to hold is that T_i be large compared to T_m so that $\left[\left(\frac{dT}{dR}\right)_{abs}\Big|_{T_i}\right]$ may remain constant during the averaging process over the variable T'. This condition no longer holds as the region of low pion energy is approached, for the value of T_i approaches the value of T_m. As a result, Eq. (7) cannot be applied to this low-energy region without some modification to take account of the variation of $\left[\left(\frac{dT}{dR}\right)_{abs}\Big|_{T_i}\right]$ or $\left[\left(\frac{dT}{dR}\right)_{em}\Big|_{T_i}\right]_{col}$ during the averaging process covering the range of T'. For the low-energy data as given in the tables of this report, it was assumed that an average of the variation of $\left[\left(\frac{dT}{dR}\right)_{abs}\Big|_{T_i}\right]$ over an energy interval corresponding to that defined by the scanning area (for the energy T_i), was a good approximation for $\left[\left(\frac{dT}{dR}\right)_{abs}\Big|_{T_i}\right]$ in Eq. (7). It was never stated[2, 5, 19] whether or not this variation of the stopping power at low energies was considered in the treatment of the data in the two other experiments.

Another effect that may influence the data is the large error that is introduced in locating the proper scanning region at low energies. As was pointed out, for monoenergetic mesons of low energy, the experimental range at which the maximum of the pion distribution occurs is shifted considerably from the actual calculated mean range--a value that was used in the other two experiments. Although in both cases a possible "flat distribution" may be expected because of the poor-geometry conditions, nevertheless this effect may introduce an error, varying in degree, in the reported cross sections in all three experiments at these low energies.

An effect that may seriously influence the low-energy cross sections as reported in the other two experiments arises from the presence

of a large background. One would judge from the nature of those experiments that no provisions were made to shield the surface of the absorber containing the emulsions from high-energy or low-energy background. In those experiments the presence of low-energy background considerably decreased the pion-to-background ratio in the scanned emulsion as compared with this ratio in the emulsions obtained with the pair magnet. Furthermore, the presence of high-energy background introduced the possibility of pion production in the absorber containing the emulsion. Even though the number of high-energy protons in such background may be small, nevertheless, the large solid angle that this possible source of pion production subtends at the emulsion does indicate that the effect may not be negligible.

To summarize: the estimated values for the cross section for pion production from the other two experiments were used to determine the value of K in Table VII at the lowest reported pion energy. For these one obtained $K < 0.5$. On the basis that the solid angle of the spiral-orbit spectrometer is constant, and from these other considerations, one may conclude that the value for the lowest pion energy as reported in Table II is probably the best value at this energy.

B. Production of Negative Pions at 90° to the Proton Beam

These two groups of experimenters [19, 5, 2] have also contributed to our knowledge on pion production information dealing with the production of negative pions from carbon at 90° to the proton beam. As some of their results are presented in plotted form, and as their interpretation of the shape of the π^- -production spectrum from carbon at 90° to the proton beam differs considerably from that presented in Fig. 16, it is important to re-examine the three experiments on π^- production from carbon. Block, et al., [2] indicate that the production cross section for negative pions at 90° to a 381-Mev proton beam is zero for zero pion energy, and gradually increases to a peak at a pion energy of approximately 38 Mev. The shape of their π^- spectrum was based on 29 observed π^- star-forming mesons. Richman and Wilcox [19, 5] have indicated a flat distribution for a pion energy between 20 and 50 Mev for the π^- -production cross section from carbon at 90° to a 340-Mev proton beam. They do not estimate the

behavior of the π^--production cross section below 10 Mev, although they do indicate a decrease. Their data were based on 48 star-forming negative pions. As seen in Fig. 16, this peaking of the π^- cross section has not been observed in this experiment. Furthermore the π^- spectrum presented in this report has its largest value at the lowest observed pion energy. The disagreement between spectral shapes in the three experiments is easily accounted for: from a statistical point of view any shape that depends on so few events as in the two earlier experiments has very little meaning.

To aid our present understanding of the possible behavior of the π^--production cross section from carbon at lower energies than reported in this experiment, and also to illustrate the possible error that may have been introduced in obtaining the integrated cross section $\left(\frac{d\sigma^-}{d\Omega}\right)_{a,\,b,\,c}$ at 90° to the proton beam, it is important to introduce data on low-energy π^- production from other elements. Preliminary results[40] on π^- production from complex nuclei at 90° to the proton beam have shown that for a pion energy as low as 12.5 Mev the relative yield of negative pions is nearly proportional to the number of neutrons in the nucleus. Some of these preliminary results are presented in Fig. 20. From these results one may argue, on the basis of the possible effect of the Coulomb barrier on π^- emission from the nucleus, that the cross section for π^- production from carbon at 90° to the proton beam may continue to increase for pion energies somewhat lower than the lowest reported energy in Fig. 16. The conclusion that this may not continue to increase as the pion energy approaches zero, but may peak and probably decrease, is justified by the shape of the π^- production spectrum at 0° (Fig. 6).

One can see from the plot in Fig. 16 that the value of the integrated cross section $\left(\frac{d\sigma^-}{d\Omega}\right)_{90^\circ}$ is greatly influenced by the assumption made on the behavior of the cross section in this low-energy region. For the calculation of the reported value it was assumed that a peak occurs at a pion energy of approximately 10 Mev and that the cross section gradually decreases. In the calculation of both the 0° and the

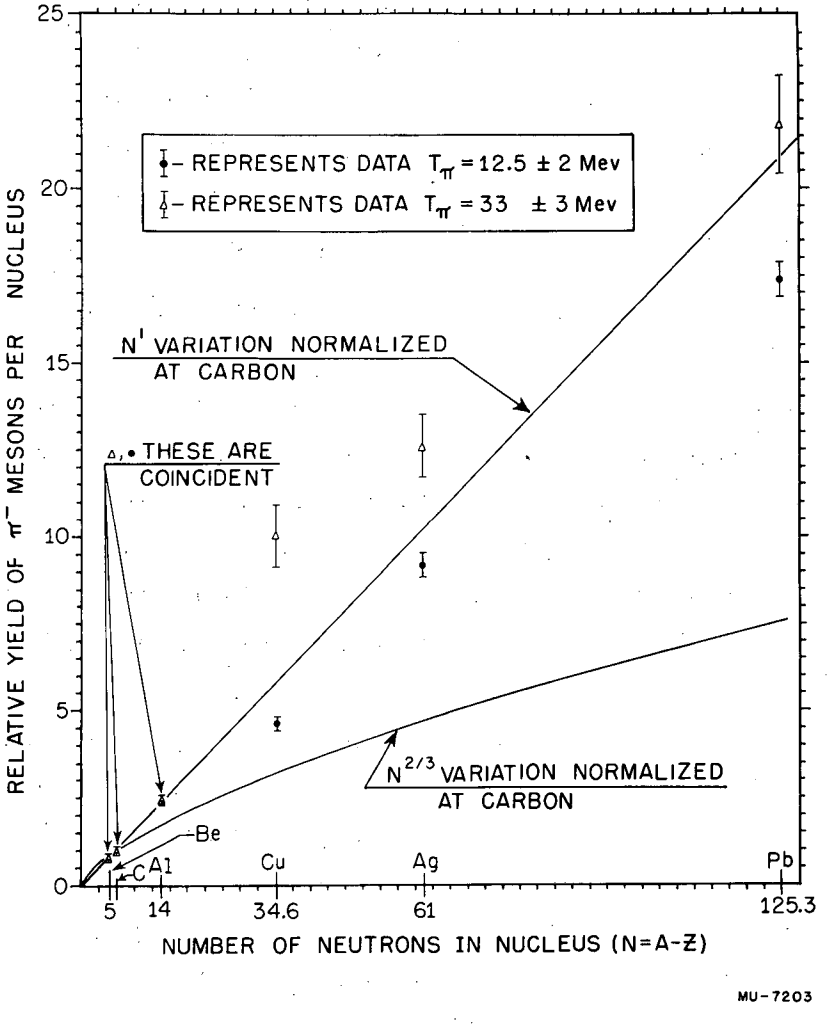

Fig. 20. Variation of negative-pion production cross sections with neutron number in the nucleus at a constant pion energy.

90° integrated π^- cross sections the assumption was made that the π^--production cross section does not go to zero for a pion of zero energy. It should also be mentioned that although there is disagreement between the shape of the spectrum for π^- production at 90° to the proton beam as presented in this report and that which is reported in the earlier experiment of Richman and Wilcox,[19, 5] the values of the integrated π^- cross section are in good agreement, as is shown by a comparison between their reported value of $(4.5 \pm 1.3) \times 10^{-29}$ cm^2 steradian^{-1}nucleus^{-1} and that given in Table VIII.

C. Our Present Knowledge About Charged-Pion Production from Carbon by 340-Mev Protons

It is worth while to mention two other published experiments[35, 38] on charged-pion production from carbon by protons so that a summary can be made of our present knowledge on pion production from this element. It is well known that pion production from an element varies with the energy of the incident proton. Such a study on the dependence of positive-pion production from carbon at 90° to the beam on proton energy has been reported by Hamlin[35]. From five observed proton energies between 235 Mev and 340 Mev he reports that the excitation function of positive-pion production is best expressed in the relation

$$Y(T_p) \sim (T_p - 150)^b \ ,$$

where $b = 2.5 \pm 0.6$ and T_p is the incident proton energy.

The second experiment reported by Leonard[38] presents data on positive and negative pion production from carbon at 180° to a 340-Mev proton beam. As this experiment was conducted on the same basis as the poor-geometry experiment that is presented in this report, one can utilize Leonard's data to obtain an estimate of the total production cross section for positive and negative pions from carbon. Some of the cross sections reported in Leonard's experiment are compared with the cross sections presented in this report in Fig. 21. An estimate of the total cross section for π^+ production from carbon can be obtained by assuming that the angular dependence of the cross section at each angle θ, integrated over pion energies, can be represented by the following relation:

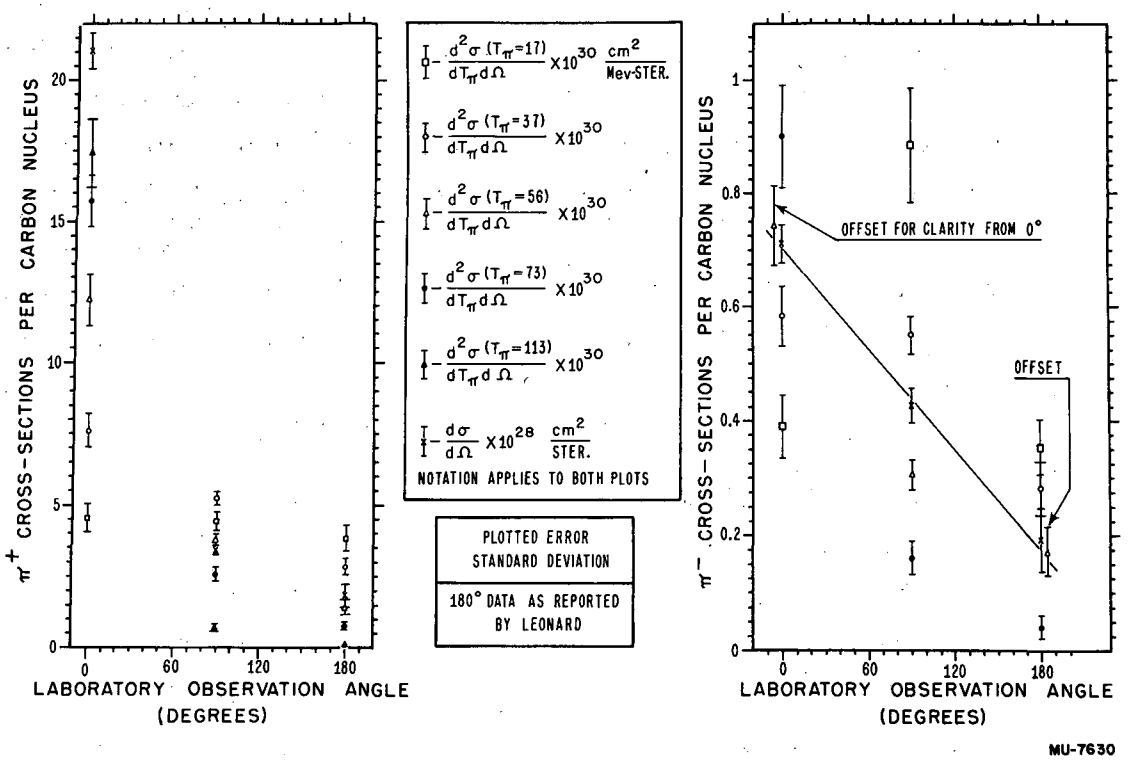

Fig. 21. Variation of pion-production cross sections from carbon with laboratory angle.

$$\frac{d\sigma^{+}(\theta)}{d\Omega} = A + B\cos\theta + C\cos^2\theta \quad .$$

When this relation is integrated over all possible laboratory angles one obtains

$$\sigma_T^{+} = 4\pi \left[A + C/3\right] = (7.6 \pm 0.7) \times 10^{-27} \text{ cm}^2 \quad ,$$

which is the estimated total production cross section for positive pions from carbon. Similarly, if one assumes the expression

$$\frac{d\sigma^{-}(\theta)}{d\Omega} = A' + B' \sin^2\theta + C' \cos\theta$$

as the angular dependence of the integrated cross section for negative pions at each laboratory angle θ, one can integrate this expression over all laboratory angles to obtain

$$\sigma_T^{-} = 4\pi \left[A' + \frac{2B'}{3}\right] = (0.55 \pm 0.09) \times 10^{-27} \text{ cm}^2$$

for the total production cross section of negative pions from carbon. In all three cases the reported error is the statistical probable error. One can now summarize what is at present expected to be the more accurate data on charged-pion production from carbon by 340-Mev protons. This summary is presented in Table XI.

As a final note it might be mentioned that any explanation of the presented results should take into consideration the effect of the nuclear Coulomb barrier on pion production. All previously proposed models do not take into account this nuclear Coulomb barrier effect. That this effect is significant is illustrated in Fig. 22, where relative yield curves[39] for positive-pion production at the same pion energy are presented as a function of atomic number. It is not being proposed that the results in Fig. 22 are entirely due to retardation of low-energy pion production by the nuclear Coulomb barrier. The curves are presented as an illustration of the significance of this effect. Furthermore, calculations have shown[46] that the Coulomb barrier may affect charged-pion production even at pion energies above 35 Mev.

In an endeavor to interpret these results one should not discount the possibility that the large π^{+}/π^{-} production ratios resulting from collisions of protons with complex nuclei may be accounted for by analogy with a similar mode of pion production: that which is found

to exist and to explain the sharp π^+ production peak resulting from free proton-proton collisions.[1, 20] That this mode of pion production is possible is illustrated in Fig. 23. This figure is a photograph of a cloud chamber in which a π^- meson is produced during a neutron-oxygen collision.[47] Emitted along with the negative pion is a deuteron.

Table IX

Summary of Results on Charged-Pion Production from Carbon by 340-Mev Protons

Measurement	π^+	π^-	π^+/π^-
$\frac{d\sigma\ (0^\circ)}{d\Omega} \times 10^{28}$ $\frac{cm^2}{Ster\text{-}nucleus}$	21.04 ± 0.50	0.714 ± 0.022	29.5 ± 1.2
$\frac{d\sigma\ (90^\circ)}{d\Omega} \times 10^{28}$ $\frac{cm^2}{Ster\text{-}nucleus}$	3.35 ± 0.07	0.427 ± 0.020	7.84 ± 0.40
$\frac{d\sigma\ (180^\circ)}{d\Omega} \times 10^{28}$ * $\frac{cm^2}{Ster\text{-}nucleus}$	1.77 ± 0.27	0.190 ± 0.038	9.3 ± 2.3
Estimated total cross section $\sigma_T \times 10^{27}$ cm^2	7.6 ± 0.7	0.55 ± 0.09	14 ± 4
Excitation function at 90° **	$Y(T_p) \sim (T_p - 150)^{2.5}$	. . .	. . .

* From Leonard's Results
** From Hamlin's Results

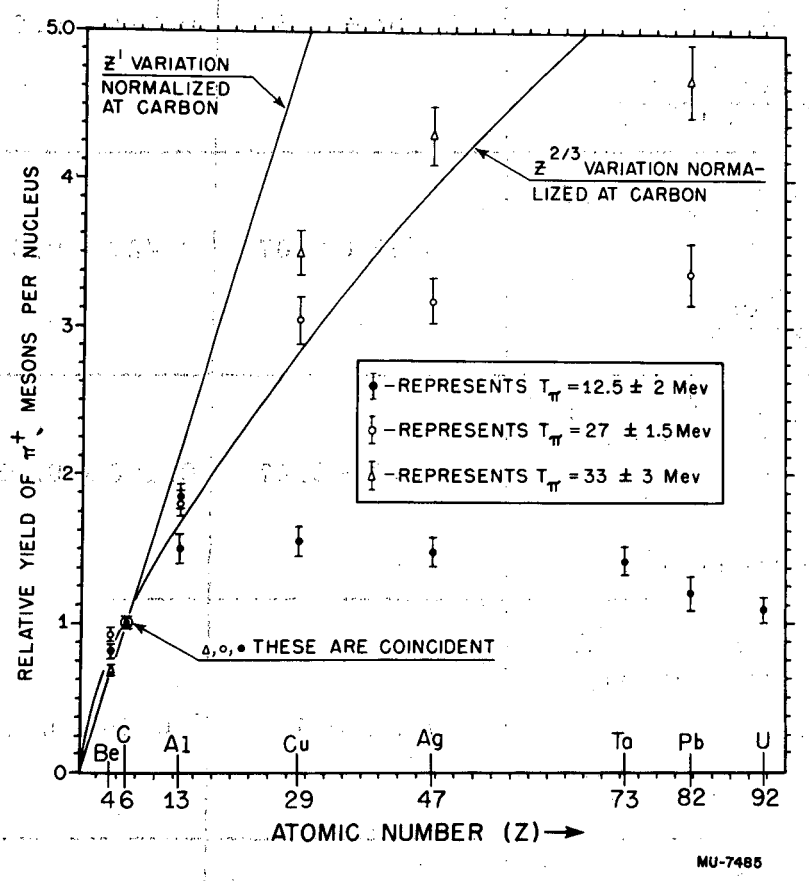

Fig. 22. Variation of positive-pion production cross sections with atomic number at a constant pion energy.

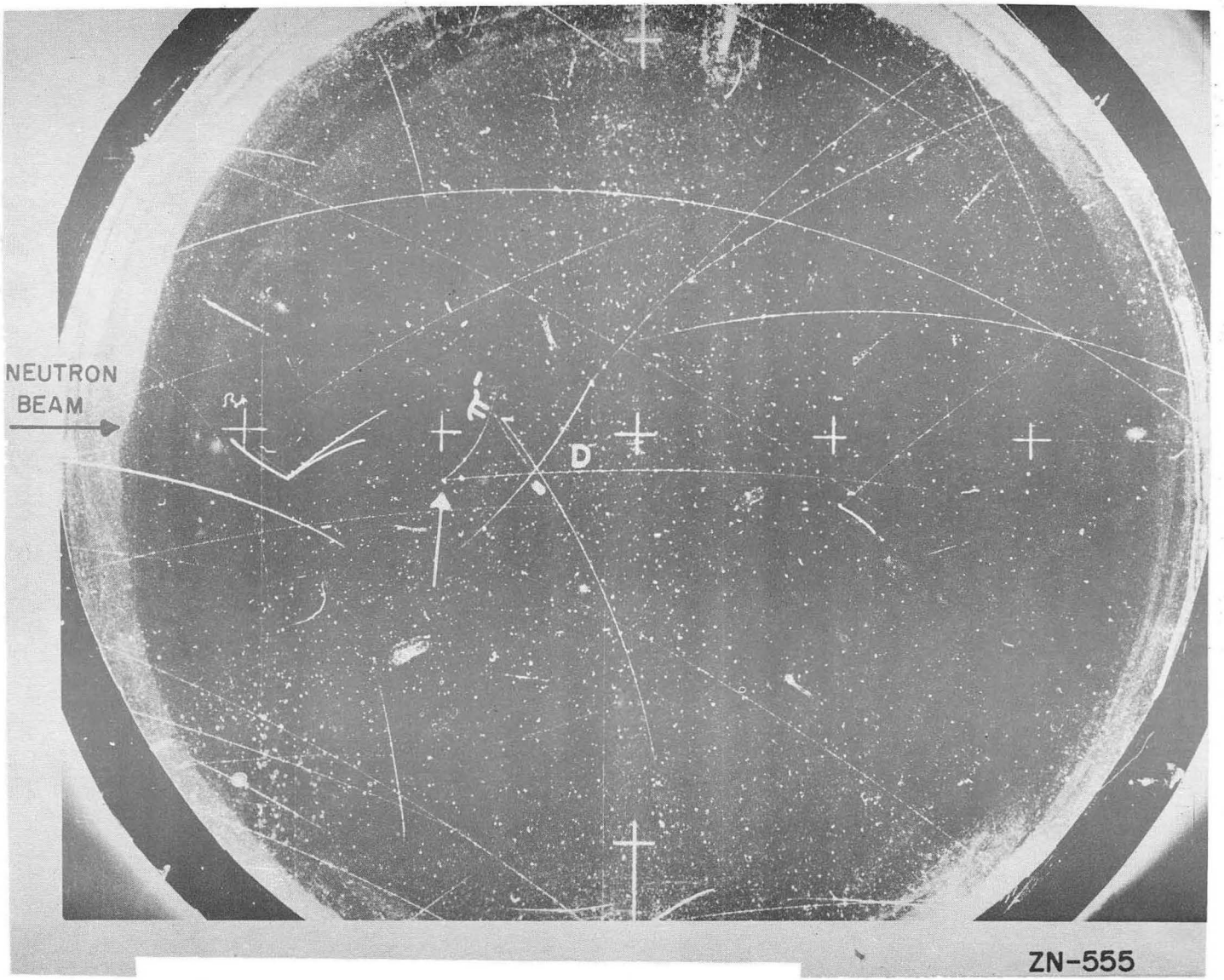

Fig. 23. Cloud-chamber photograph illustrating a neutron-oxygen collision resulting in the emission of negative pion and a deuteron.

ACKNOWLEDGMENTS

It is difficult in a brief summary to justly acknowledge the help of everyone at the Radiation Laboratory and the Physics Department of the University of California who played a part in molding the ideas that have led to these studies. This list would surely be a lengthy one. To all of those who are not mentioned I apologize, for to all I am equally indebted.

It is a pleasure to express my sincerest appreciation to Professor Chaim Richman, who introduced me to the field of meson physics and who first suggested the π^- experiment at 0°. From this, and through his encouragement and guidance, stemmed many of the ideas that are summarized in this paper.

Similarly it is my great pleasure to express my sincere appreciation to Dr. Ryokichi Sagane, with whose aid most of the spiral-orbit measurements were made. To him I owe my present understanding of the spiral-orbit principle. Although throughout the studies with the spiral-orbit spectrometer we worked on the same level, I still feel our relationship is that of grateful student to helpful professor.

I would like to express my appreciation to Professor Robert Thornton, who must be credited with obtaining the funds for the construction of the 22-inch spiral-orbit spectrometer.

I am equally grateful to Dr. Donald Stork for his aid during the early stages of the poor-geometry experiment, and also to Mr. James Vedder for his aid during the spiral-orbit experiments.

It is only fitting to mention among all of these the two who were most responsible, as it was only through their sacrifice and effort that my ambition could be realized. For this I shall always be indebted to Mother and Dad.

This work was done under the auspices of the Atomic Energy Commission.

APPENDIX

Proton Energy and Proton Monitor

The incident-proton beam intensity fluctuates during each exposure, as the bombarding time for each exposure is long (from 3 to 9 hours). For some exposures the beam intensity varied by as much as a factor of two. Because of this fluctuation, the proton monitoring system that measures the number of protons in the incident beam, (N_p or I_p), can greatly influence not only the shape of the reported spectrum, but also the accuracy of each measurement. A calibration was made to check the behavior of the proton-monitoring system.

The proton monitor was a shallow parallel-plate ionization chamber (Fig. 24a) through which the incident beam passed prior to reaching the target. The chamber was filled with argon to approximately 4 cm Hg above atmospheric pressure. The ionization produced in the ionization chamber was measured by collecting it in a condenser and measuring the potential across the condenser with a 100% inverse-feedback electrometer (Fig. 24b).

Figure 25a illustrates the calibration arrangement. The current in the beam was measured first by two ionization chambers of the type shown in Fig. 24a, and then by a Faraday cup, which is the primary standard for determining the beam intensity. The Faraday cup consists of a 6-by-6-inch copper cylinder supported by Teflon insulators as shown in Fig. 25b. Across the face of the Faraday cup is a bias foil that is used to test for the effect of secondary electron emission from the electrode. The whole Faraday-cup structure is in an evacuated enclosure. A magnetic field of 100 gauss across the face of the Faraday cup serves to greatly reduce the secondary electron emission. As shown in Fig. 26b, a change of bias-foil potential of 430 volts caused a change in the apparent calibration of the ionization chamber of less than 1%. This indicated that the secondary electron emission was satisfactorily small. The apparent multiplication factor M' of the ionization chamber appearing in Fig. 26b is defined as the ratio between the saturated current collected in the ionization chamber and the corresponding current collected in the Faraday cup. In order to compare the experimental results that were monitored by

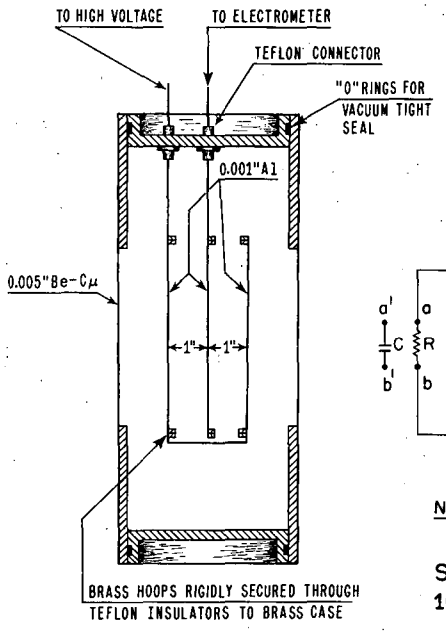

SCHEMATIC DIAGRAM OF THE PARALLEL PLATE IONIZATION CHAMBER.

(a)

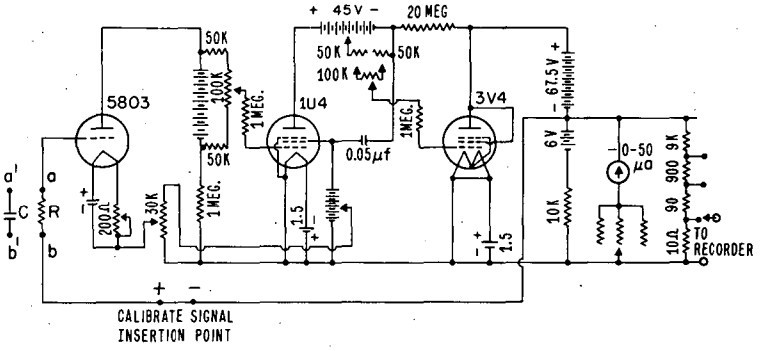

NOTE: C IS USED FOR INTEGRATING ELECTROMETER
R IS USED FOR CURRENT ELECTROMETER

SIMPLIFIED SCHEMATIC DIAGRAM OF THE 100 PER CENT INVERSE FEEDBACK INTEGRATING ELECTROMETER.

(b)

MU-7508

Fig. 24.

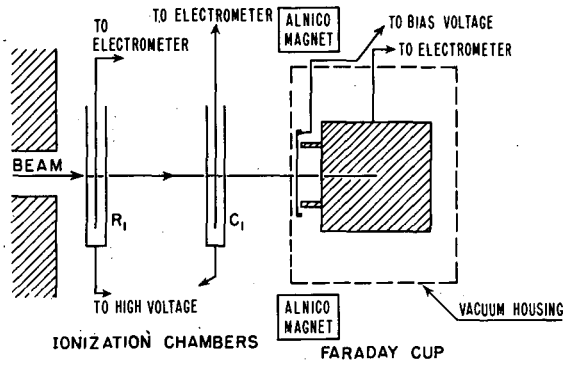

SCHEMATIC DIAGRAM OF CALIBRATION ARRANGEMENT.

(a)

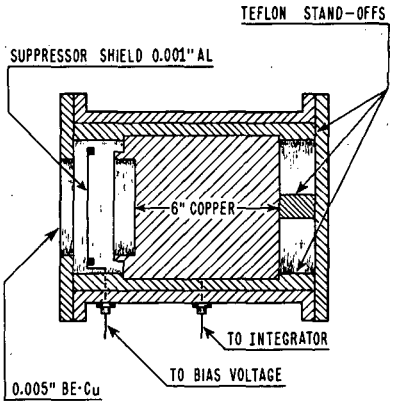

CROSS-SECTION OF FARADAY CUP.

MU-7490

(b)

Fig. 25.

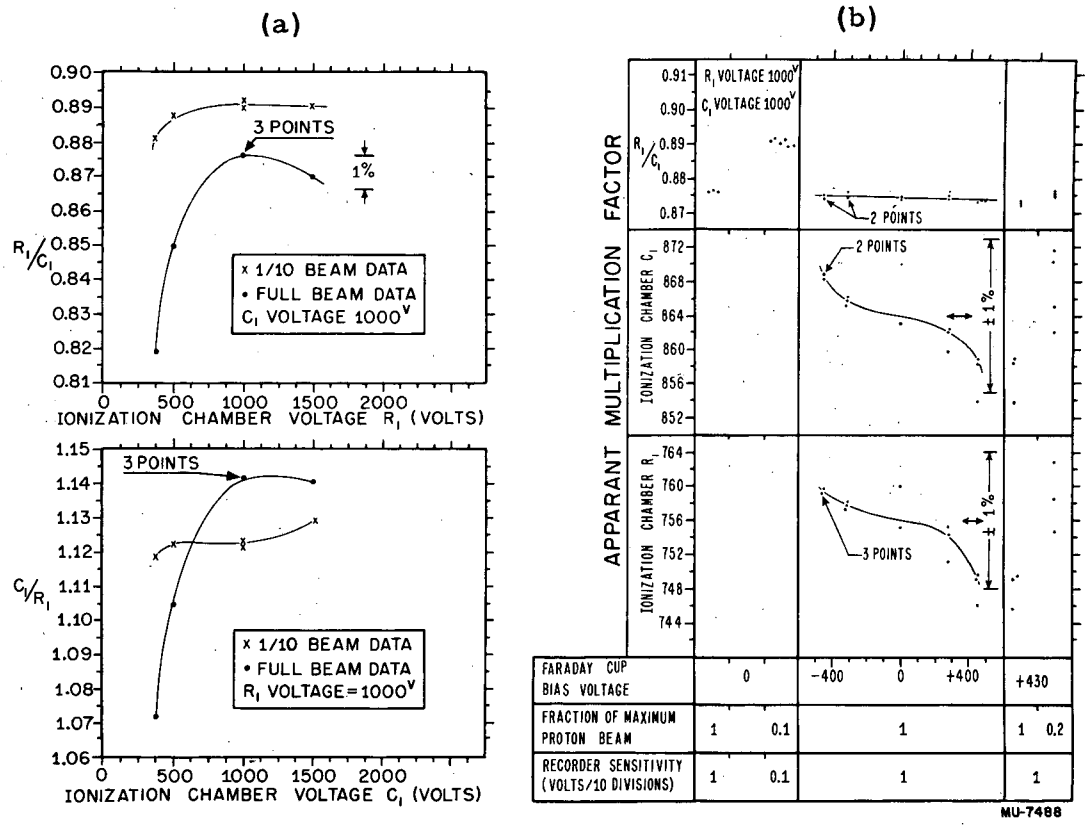

Fig. 26. Results of calibration of a ||-plate ionization chamber for (a) the saturation effect with beam intensity, (b) apparent multiplication factor with beam intensity and Faraday cup bias voltage.

either of the two ionization chambers, five corrections were applied to the apparent multiplication factor to obtain the multiplication factor M that was used during the experiment. These corrections and their values are presented in Table X.

Table X

Corrections Applied to the Apparent Multiplication Factor

Ionization Chamber		R_1	C_1
Faraday cup screen voltage		1.009	1.008
Condenser calibration		1.063	0.951
Pressure		1.290	1.299
Plate separation		0.998	0.986
Electrometer sensitivity	0.01	1.008	1.012
	0.1	0.997	0.987
Net correction	0.01	1.392	1.243
	0.1	1.377	1.212
Multiplication factor M	at full beam	1042	1067
	at 1/5 full beam	1053	1074

The value M in Table X is the multiplication factor that is obtained for a shallow parallel-plate ionization chamber filled with argon to an absolute pressure of 100 cm Hg at 20°C, having 2.000 inches for the plate separation and corrected to a zero bias-screen voltage of the Faraday cup.

As seen in Table X, the multiplication factor does change with proton beam intensity. Because of this small change in the value of M at the two vastly different beam intensities, no correction for the saturation effect of the ionization chamber was applied to the reported cross sections for the intensity fluctuations that were observed during the experiment. This is justified since the ionization chamber was operated in the saturated region for all beam intensities during the experiment, as shown in Fig. 26a.

Immediately following one part of these experiments, the energy of the proton beam was measured by Dr. R. Mather with his Cerenkov radiation method.[48] The value of this measured energy was 340 Mev. To check the constancy of this energy a portion of the projected range curve in copper, as shown in Fig. 27, was obtained intermittently. Within experimental error the results from this portion of the Bragg curve were within 1/2% of being the same. This excellent check on the constancy of the proton energy is not surprising. As seen in Fig. 1a, the deflecting apparatus of the 184-inch synchrocyclotron assures a well-collimated, nearly monoenergetic beam by the time the protons reach the experimental area. A slight change in energy results from the complete readjustment of the controls after intervening duty on other experiments.

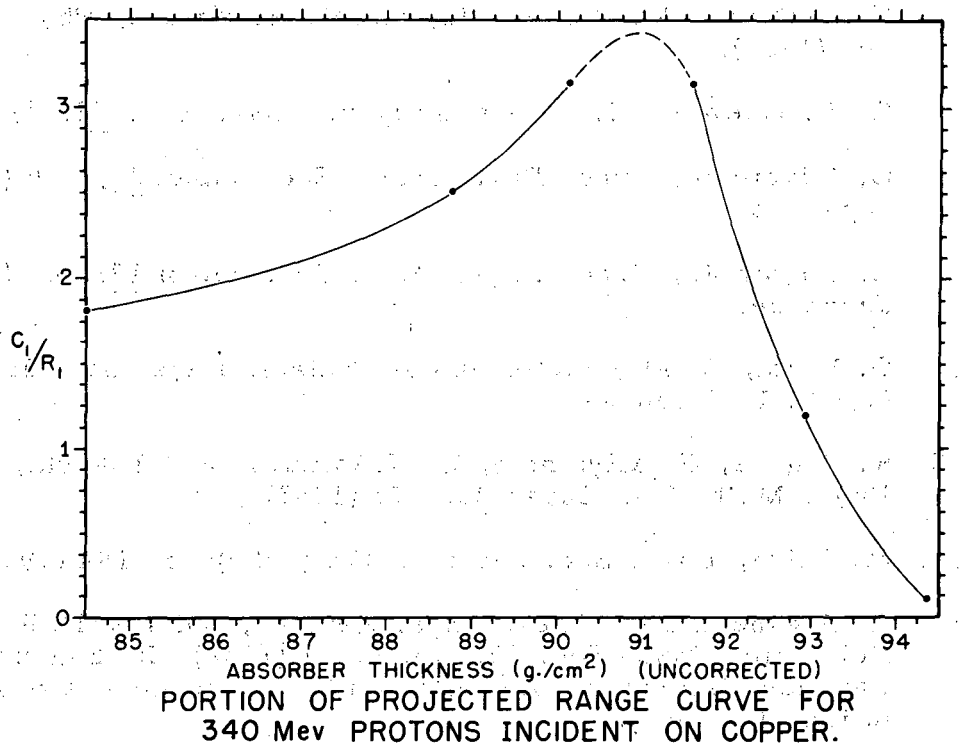
3
2
1
0
C_1/R_1
85
86
87
88
89
90
91
92
93
94
ABSORBER THICKNESS (g./cm^2) (UNCORRECTED)
PORTION OF PROJECTED RANGE CURVE FOR
340 Mev PROTONS INCIDENT ON COPPER.
MU-7506

Fig. 27.

REFERENCES

1. W. F. Cartwright, C. Richman, M. N. Whitehead, and H. A. Wilcox, Phys. Rev. 91, 677 (1953); A. G. Shulz, Jr., (Thesis) University of California Radiation Laboratory Report No. UCRL-1756, May 1952.

2. S. Passman, M. M. Block, and W. W. Havens, Jr., Phys. Rev. 88, 1247 (1952); M. Block, S. Passman, and W. Havens, Jr., Phys. Rev. 88, 1243 (1952).

3. W. F. Dudziak, Bull. Am. Phys. Soc. 29, No. 1, 19 (1954) (to be published in Phys. Rev.)

4. W. F. Dudziak, Phys. Rev. 86, 602 (1952).

5. C. Richman, M. Weissbluth, and H. A. Wilcox, Phys. Rev. 85, 161 (1952).

6. G. F. Chew and J. L. Steinberger, Phys. Rev. 78, 497 (1950).

7. G. Miyamoto, Proc. Phys. Math. Soc. Japan 24, 676 (1942). In Japanese.

8. G. Miyamoto, Proc. Phys. Math. Soc. Japan 17, 587 (1943). In Japanese.

9. G. Iwata, G. Miyamoto, and M. Kotani, Phys. Soc. Japan 2, 1 (1947). In Japanese.

10. R. Sagane, G. Miyamoto, K. Nakamura, and Takechi, Pros. Phys. Math. Soc. Japan 25, 274 (1943).

11. M. Sakai, Phys. Soc. Japan 5, 178 (1950); 5, 184 (1950).

12. R. Sagane and P. Giles, Phys. Rev. 81, 653 (1951); R. Sagane, Bull. Am. Phys. Soc. 27, No. 6, 17 (1952); R. Sagane and W. Gardner, University of California Radiation Laboratory Translation 111 (1951).

13. R. Sagane, Phys. Rev. 90, 1003 (1953).

14. W. F. Dudziak, Phys. Rev. 90, 342 (1953).

15. C. Richman, private communication.*

16. Occhialini and Powell, Nature, Lond. 162, 168 (1948).

17. F. Adelman and S. Jones, Science 111, 226 (1950); M. Menon, H. Muirhead, O. Rochat, Phil. Mag. 41, 583 (1950).

*Although the reported expression in Ref. 5 is identical with Ref. 2, the actual cross sections were calculated with formula reported in Ref. 1.

18. Powell, Henrich, Kerns, Sewell, and Thornton, Rev. Sci. Instr. 19, 506 (1948).

19. C. Richman and H. Wilcox, Phys. Rev. 78, 496 (1950).

20. W. Cartwright, C. Richman, M. Whitehead, and H. Wilcox, Phys. Rev. 78, 823 (1950).

21. L. Eyges, Phys. Rev. 74, 1534 (1948).

22. R. R. Wilson, Phys. Rev. 71, 385 (1947).

23. W. F. Cartwright, Production of π^+-Mesons by 340-Mev Protons on Protons at 0° to the Beam (Thesis), University of California Radiation Laboratory Report No. UCRL-1278, April 1951.

24. W. A. Aron, The Passage of Charged Particles through Matter (Thesis), University of California Radiation Laboratory Report No. UCRL-1325, May 1951.

25. R. Sagane, Employment of the Spiral-Orbit Spectrometer to Measure Pion Production Ratios by Proton Bombardment, University of California Radiation Laboratory Report No. UCRL-2161, (1953).

26. M. Jakobson, A. Schulz, J. Steinberger, Phys. Rev. 81, 894 (1951). (π^+ mean life)

27. R. Durbin, H. Loar, W. Havens, Jr., Phys. Rev. 88, 179 (1952). (π^- mean life)

28. H. Bradner, F. Smith, W. Barkas, and A. Bishop, Phys. Rev. 77, 462 (1950).

29. H. Byfield, J. Kessler, and L. M. Lederman, Phys. Rev. 86, 17 (1952).

30. D. Stork, Phys. Rev. 93, 868 (1954); R. Martin, Phys. Rev. 87, 1052 (1952); H. Bradner and B. Rankin, Phys. Rev. 80, 916 (1950); C. Chedester, P. Isaacs, A. Sachs, and J. Steinberger, Phys. Rev. 82, 958 (1951); G. Bernardini, E. Booth, L. Lederman, and J. Tinlot, Phys. Rev. 80, 924 (1950).

31. D. H. Perkins, Phil. Mag. 40, 601 (1949); W. Cheston and L. Goldfarb, Phys. Rev. 78, 683 (1950); F. L. Adelman, Phys. Rev. 85, 249 (1952).

32. R. Sagane, W. F. Dudziak, and J. Vedder, Phys. Rev. (to be published).

33. Landau and Lifshitz, Classical Theory of Fields, Addison-Wesley Press, 1951, p. 42; Bergman, Introduction to the Theory of Relativity, Prentice-Hall, 1942, p. 117.

34. H. B. Keller and C. Dols, Extending the Range of a Self-Balancing Recording Potentrometer without Reducing Resolution, University of California Radiation Laboratory Report No. UCRL-2049 (rev.), January 1954.

35. D. Hamlin, Excitation Function for Positive Pions Produced at 90° in Proton-Carbon Collisions (Thesis), University of California Radiation Laboratory Report No. UCRL-2414, November 1953.

36. L. Vigneron, J. de Physique, 14, 157 (1953). In French.

37. R. M. Sternheimer, Phys. Rev. 88, 851 (1952).

38. S. Leonard, Phys. Rev. 93, 1380 (1954).

39. R. Sagane and W. F. Dudziak, The Dependence of the 33-Mev π^+-Production Cross Sections on Atomic Number, University of California Radiation Laboratory Report No. UCRL-2284, July 1953; Dependence of Positive-Pion Production Cross Sections on Atomic Number at Low Energies, University of California Radiation Laboratory Report No. UCRL-2317, September 1953; Phys. Rev. 92, 212 (1953).

40. W. F. Dudziak and R. Sagane, The Dependence of Negative Pion Production on Neutron Number, University of California Radiation Laboratory Report No. UCRL-2304, August 1953.

41. M. Livingston and H. Bethe, Revs. Modern Phys. 9, 285 (1937).

42. H. Bradner, F. Smith, W. Barkas, and A. Bishop, Phys. Rev. 77, 462 (1950).

43. W. Barkas, Private Communication.

44. O. Heinz, Range and Specific Ionization for High-Energy Protons in Nuclear Emulsions, University of California Radiation Laboratory Report No. UCRL-2458, January 1954.

45. D. Hamlin, Private Communication.

46. T. Kinoshita, Private Communication (to be published in Phys. Rev.).

47. Courtesy of Dr. F. Ford; also, F. Ford, The Production of Charged π Mesons by Neutrons on Oxygen (Thesis), University of California Radiation Laboratory Report No. UCRL-2148, March 1953.

48. R. Mather, Phys. Rev. 84, 181 (1951).